
Membership Inference Risks in Quantized Models: A Theoretical and Empirical Study

Eric Aubinais^{*12} Philippe Formont^{*134} Pablo Piantanida¹³⁴⁵ Elisabeth Gassiat¹²

Abstract

Quantizing machine learning models has demonstrated its effectiveness in lowering memory and inference costs while maintaining performance levels comparable to the original models. In this work, we investigate the impact of quantization procedures on the privacy of data-driven models, specifically focusing on their vulnerability to membership inference attacks. We derive an asymptotic theoretical analysis of Membership Inference Security (MIS), characterizing the privacy implications of quantized algorithm weights against the most powerful (and possibly unknown) attacks. Building on these theoretical insights, we propose a novel methodology to empirically assess and rank the privacy levels of various quantization procedures. Using synthetic datasets, we demonstrate the effectiveness of our approach in assessing the MIS of different quantizers. Furthermore, we explore the trade-off between privacy and performance using real-world data and models in the context of molecular modeling.

1. Introduction

Reducing the computational and memory costs of machine learning models is a critical aspect of their deployment, particularly on edge devices and resource-constrained environments. Quantization stands out among the various methods available to enhance inference efficiency in neural networks, such as knowledge distillation and pruning, due to its distinct advantages and proven practical success (Gholami et al., 2022). One key benefit is that the storage and latency improvements achieved through quantization are

deterministically defined by the chosen quantization level (e.g., using 8-bit integers instead of 32-bit floating-point numbers). Moreover, uniform quantization is inherently hardware-friendly, facilitating the practical realization of theoretical efficiency gains.

While quantization effectively improves efficiency, its impact on the privacy of machine learning models remains largely under-explored. A particularly intriguing question is whether quantization can also strengthen a model’s resilience against adversarial threats, such as the extraction of sensitive information. By reducing the precision of a model’s parameters, quantization naturally discards some information (Villard & Piantanida, 2013), which leads to the hypothesis that this process could potentially reduce the risk of recovering the model’s training data or other private information. However, to our knowledge, the security of quantized models against such privacy attacks has not yet been theoretically investigated.

In this paper, we explore the effect of quantization on the Membership Inference vulnerability of machine learning models. We propose a novel privacy metric, based upon the Membership Inference Security (MIS) (Aubinais et al., 2023) and derive asymptotic bounds—relative to the training sample size—to quantify the privacy implications of model quantization. Using these theoretical insights, we present a systematic framework for evaluating and comparing fundamental quantization techniques, with a focus on the observed loss values. This methodology provides a thorough analysis of how different quantization methods strike a balance between privacy (against the most powerful attacks) and performance. To validate our approach, we compare it against an established baseline technique, showing consistent rankings of quantization methods based on their ability to preserve privacy.

1.1. Our contributions

Our contributions can be summarized as follows:

- We show that, for a fixed model and quantization procedure, as the size of the training dataset increases towards infinity, the MIS of the learning algorithm is fully determined by the distribution of the loss per sam-

^{*}Equal contribution ¹Université Paris-Saclay ²Laboratoire de mathématiques d’Orsay, France ³Ecole de technologie supérieure, ILLS - International Laboratory on Learning Systems, Montreal, Canada ⁴MILA - Quebec AI Institute, Montreal, Canada ⁵CNRS, CentraleSupélec. Correspondence to: Philippe Formont <philippe.formont@mila.quebec>, Eric Aubinais <eric.aubinais@universite-paris-saclay.fr>.

ple for the quantized models (Theorem 3.1). Building upon this result, we further show that when the model architecture and/or quantization procedure adapts to the training set size, a similar dependency persists (Theorem 3.3), although with a more precise dependence on the covariance structure of the loss per sample.

- Building on the result of Theorem 3.3, whose direct estimation is computationally prohibitive, we propose a methodology (subsection 4.1) enabling the comparison of quantizers in terms of privacy.
- We apply our methodology to several Post-Training Quantization techniques on both synthetic data (see Figure 5) and real-world data (see subsection 5.2). We show that the rankings provided by our method consistently correlates with the ones obtained with a baseline estimation of the MIS (see subsection 5.1.2), and study the privacy-performance trade-off of quantization on molecular property prediction tasks (see subsection 5.2.2).

Our work is dedicated to providing a theoretically grounded methodology to compare different quantization procedures in the context of MIS evaluation.

1.2. Related work

Quantization of neural networks. With the deployment of neural networks on edge devices (Yuan et al., 2024; Lin et al., 2024), where inference should be time and memory efficient, several quantization procedures have been studied and employed. Quantization usually answers this task by reducing the (bit-)precision of the parameters of the neural networks, demonstrating effectiveness in Large Language Models (Gong et al., 2024; Zhu et al., 2024) even when the quantization is as strong as 1-bit precision quantization (Wang et al., 2023; Ma et al., 2024a), 1.58-bits precision quantization (Ma et al., 2024b), arbitrary bits precision (Zeng et al., 2024). The most adopted framework of quantization is Post-Training Quantization (PTQ) (Jacob et al., 2018; Nagel et al., 2019; Gholami et al., 2022) which provides simple training-free implementation. PTQ is usually adopted over Quantization-Aware Training (QAT) (Bengio et al., 2013; Banner et al., 2018; Nagel et al., 2021; 2022; Pang et al., 2024) due to their limitations to scale up to larger models (Gholami et al., 2022; Lin et al., 2024). Additionally, some lines of work study "hardware-aware" quantization procedures (Wang et al., 2024; Balaskas et al., 2024) where optimization is made directly on the hardware. During our experiments, we will focus on PTQ.

Membership Inference Attacks. Membership Inference Attacks (MIAs) can reveal sensible information (Shokri et al., 2017; Song et al., 2017; Carlini et al., 2022; 2023) about one’s data by leveraging the information stored in the

parameters of the ML model (Hartley & Tsafaris, 2022; Del Grosso et al., 2023). An extensive line of work has developed in the past decade to construct ever so powerful MIAs in embedding models (Song & Raghunathan, 2020), regression models (Gupta et al., 2021) or generative models (Hayes et al.), systematically summarized in (Hu et al., 2022). Recent works have leveraged the predictive power of LLMs to construct new MIAs (Staab et al., 2023; Wang et al., 2025). While few works have delved into the theoretical intricacies of MIAs (Sablayrolles et al., 2019; Del Grosso et al., 2023; Aubinais et al., 2023), several Privacy benchmarks have been developed to audit the privacy risks of ML models (Murakonda & Shokri, 2020; Liu et al., 2022b) by evaluating state-of-the-art MIAs on the target model. Although these benchmarks offer valuable insights into the privacy leakage of an ML model, a single MIA alone cannot provide a comprehensive assessment of an algorithm’s overall privacy resilience against various attacks. We briefly discuss it in subsection 2.3.

Quantization and Privacy. Various strategies to protect models from attacks like MIAs have been proposed. In federated learning, the effects of input and gradient quantization have been analyzed through the lens of differential privacy (Youn et al., 2023; Yan et al., 2024; Chaudhuri et al., 2022). However, the impact of model quantization on security has been primarily assessed through empirical evaluations of MIAs, with no existing theoretical analysis (Kowalski et al., 2022; Famili & Lao, 2023). Our work aims to fill this gap by providing a rigorous theoretical evaluation of the security implications of model quantization.

2. Background and Notations

2.1. Predictive tasks

Throughout the article, we consider a dataset $\mathcal{D}_n := \{z_1, \dots, z_n\}$ of n independent and identically distributed (i.i.d.) data drawn from a common distribution P over a space \mathcal{Z} . We assume that our goal is to infer a predictive function $\hat{\Psi}$ from a set of predictors $\mathcal{F} := \{\Psi_\theta : \theta \in \Theta\}$ indexed by some space $\Theta \subseteq \mathbb{R}^d$. We define a (learning) **algorithm** as a function $\mathcal{A} : \bigcup_{n \geq 1} \mathcal{Z}^n \rightarrow \mathcal{P}(\Theta)$, where $\mathcal{P}(\Theta)$ is the space of all probability measures on Θ . By denoting $\hat{\theta}_n \sim \mathcal{A}(z_1, \dots, z_n) \in \Theta$, we systematically set $\hat{\Psi} = \Psi_{\hat{\theta}_n}$. This definition of a learning algorithm includes all (stochastic) algorithms. We will assume in the following that the algorithm can be written as a function of the empirical distribution of the data. More specifically, this means that there exists a function G and a random variable ξ such that $\mathcal{A}(z_1, \dots, z_n) = G(\hat{P}_n, \xi)$, where \hat{P}_n is the empirical distribution of the training dataset. In this case, the random variable ξ encompasses the stochasticity of the algorithm. This assumption is especially satisfied for algorithms minimizing an empirical loss $\theta \mapsto \frac{1}{n} \sum_{j=1}^n \ell(\theta, z_j)$

where $\ell : \Theta \times \mathcal{Z} \rightarrow \mathbb{R}^+$ is the loss function.

Example 2.1. Classification. For a classification task, we may note $\mathcal{Z} := \mathcal{X} \times \mathcal{Y}$ where $\mathcal{Y} = \{1, \dots, |\mathcal{Y}|\}$ is the number of classes and \mathcal{X} is the input space. \mathcal{F} can be the set of all neural networks, where $\theta \in \Theta$ then represents the parameters of such predictors. The algorithm \mathcal{A} can be any (stochastic) optimizing procedure (e.g., Adam optimizer) on any adequate loss function (e.g., the cross-entropy loss).

2.2. Quantization

We define a **quantizer** (Gersho & Gray, 1992) as any measurable function $\mathcal{Q} : \Theta \rightarrow \bar{\Theta} \subseteq \Theta$ for some discrete space $\bar{\Theta} := \{\bar{\theta}_1, \dots, \bar{\theta}_K\}$. A quantizer canonically induces a **quantized algorithm** $\mathcal{A}_{\mathcal{Q}}$, and a loss function $\ell_{\mathcal{Q}}$, which we simply write ℓ , as long as there is no ambiguity. For any $\theta \in \Theta$, we denote by $m_{\theta} = \mathbb{E}[\ell(\theta, z)]$ the expected loss evaluated on θ , where z is a random variable with distribution P . Additionally, for a given quantizer \mathcal{Q} , we will assume without loss of generality that $m_{\bar{\theta}_1} \leq \dots \leq m_{\bar{\theta}_K}$. In the following, we introduce two specific examples to illustrate particular quantization methods.

Example 2.2 (Binarized Neural Networks (Wang et al., 2023)). Let \mathcal{F} be a set of neural networks with fixed architecture. The set Θ then represents the parameters of the neural network. A scalar quantizer \mathcal{Q} maps coordinate-wise the parameters to its sign, namely $\mathcal{Q}(\theta) = (\theta_j / |\theta_j|)_j$. Here, for 1-layer unbiased neural networks with width d (number of parameters), the set $\bar{\Theta}$ would consist of all d -dimensional vectors in $\{-1, +1\}^d$ where $K = 2^d$. Usually, computers store parameters in a 32-bits (or 64-bits) format. Low-precision quantization procedures, e.g. 2-bits (or q -bits in general) quantization, reduce the number of bits required from 32 (or 64) to 2 (or q in general).

Example 2.3 (Vector Quantization). Another quantization procedure, albeit under-used in practice, is vector quantization. A *codebook* $\bar{\Theta}$ is usually pre-computed, which the vector quantizer \mathcal{Q} maps θ onto, usually performed by a nearest neighbor algorithm, which makes it efficient and memory-friendly. The constant K here corresponds to the number of values stored in the codebook.

2.3. Privacy assessment

In the present work, we evaluate the privacy of an algorithm \mathcal{A} trained on a task P through Membership Inference Attacks (MIAs). Particularly, in a scenario where \mathcal{D}_n consists of sensible data and the model $\hat{\Psi}$ has been shared (such as a sold product), MIAs are known to pose a notable threat to the privacy of the dataset. MIAs aim at inferring membership of a test sample \tilde{z} to the dataset \mathcal{D}_n by observing $\hat{\theta}_n$. MIAs can be defined as follows.

Definition 2.4 (Membership Inference Attack - MIA). Any measurable map $\phi : \Theta \times \mathcal{Z} \rightarrow \{\text{member, non-member}\}$ is

considered to be a *Membership Inference Attack*.

The existence of successful MIAs constitute a major threat against the privacy of personal data by revealing sensible information. However, for most algorithms, there may always exist pathological datasets for which models trained on would be highly attackable by MIAs. Specifically, although individual MIAs can reveal information leakage, it is alone insufficient to disclose a complete overview on the privacy level of a machine learning model. To adequately tackle down the question of privacy of an algorithm, it is compulsory to address all possibilities of attacks. We then will say that an algorithm is private if it *usually* produces parameters $\hat{\theta}_n$ that are private against *most* MIAs. We use the notion of accuracy of an MIA, defined as the probability of successfully guessing the membership of the test point. Letting $T \in \{\text{member, non-member}\}$ encode the membership of a test point \tilde{z} , we define the accuracy as follows.

Definition 2.5 (Accuracy of a given MIA). The *accuracy* of an MIA ϕ is defined as

$$\text{Acc}_n(\phi; P, \mathcal{A}) := P\left(\phi(\hat{\theta}_n, \tilde{z}) = T\right), \quad (1)$$

where the probability is considered over all sources of randomness inherent in the underlying training model and the data used for both training and evaluation.

Definition 2.6 (MIS). The *Membership Inference Security* (MIS) of an algorithm \mathcal{A} is defined as

$$\text{MIS}_n(P, \mathcal{A}) := 2 \left(1 - \sup_{\phi} \text{Acc}_n(\phi; P, \mathcal{A}) \right), \quad (2)$$

where the sup is taken over all MIAs and thus, $\text{MIS}_n(P, \mathcal{A}) \leq 2(1 - \text{Acc}_n(\phi; P, \mathcal{A}))$ for all MIAs ϕ .

We notice that MIAs with an accuracy of at least $\frac{1}{2}$ always exist (e.g., constant MIAs). As a result, the MIS metric ranges from 0 (completely non-private) to 1 (fully private).

Remark 2.7. The presence of the supremum makes the MIS a metric encompassing all possible MIAs, including all state-of-the-art MIAs, and most importantly, all unknown MIAs. Indeed, even though state-of-the-art MIAs provide a strong indicator on the security of ML models, more powerful MIAs are likely to emerge in the future, beating the state-of-the-art MIAs. Consequently, it is of paramount importance to consider all attacks when designing privacy metrics.

3. Theoretical Results

We provide in this section the main theoretical results on the MIS of quantized algorithms. For the results of [section 3](#) and [section 4](#) to hold, it is mandatory to give a proper mathematical setting, although not required for the reader to pursue. We therefore refer to [subsection A.1](#) for a formal mathematical setting.

3.1. Fixed Quantizer

We start off by giving a simple result. Let \mathcal{Q} be a fixed quantizer, then under mild additional assumptions presented in subsection A.2, the following result holds.

Theorem 3.1. *There exists a constant $C_P^1 > 0$ satisfying*

$$\lim_{n \rightarrow \infty} -\frac{1}{n} \log(1 - \text{MIS}_n(P, \mathcal{A}_{\mathcal{Q}})) \geq C_P^1. \quad (3)$$

Importantly, the constant C_P^1 depends solely on the distribution of $\ell(\theta, z)$ for all $\theta \in \Theta$, where z has for distribution P . The detailed formulation of the theorem can be found in Theorem C.1. This theorem establishes that the MIS is of order $1 - e^{-nC_P^1(1+o(1))}$ for some constant $C_P^1 > 0$ for a given algorithm. The result suggests that the approximation holds as the dataset size approaches infinity, assuming the architecture size remains fixed. However, in practice, when developing machine learning models, it is common to adjust the architecture based on the dataset, particularly its size.

3.2. Size-Adaptive Quantizers

As an example, it is common to over-parameterize models relative to the dataset size, as seen in the case of LLMs. Therefore, Theorem 3.1 may not provide an accurate approximation for very large datasets. We now let our quantizer \mathcal{Q}_n (and therefore the number of quantized values K_n and $\bar{\Theta}_n := \{\bar{\theta}_1, \dots, \bar{\theta}_{K_n}\}$) be *Size-Adaptive*, i.e. depends on the sample size. Let $\delta_k^n := m_{\bar{\theta}_k^n} - m_{\bar{\theta}_1^n}$ be the **loss gaps** and $(\sigma_k^n)^2 = \text{Var}(\ell(\bar{\theta}_k^n, z) - \ell(\bar{\theta}_1^n, z))$ be the **loss variabilities**, which corresponds to the variance of the difference of the losses between $\bar{\theta}_k^n$ and $\bar{\theta}_1^n$.

The dependence of \mathcal{Q}_n on the dataset size n formalizes at least two scenarios: either the quantization procedure remains the same, but the architecture size adapts to the training dataset, or the architecture size is fixed while the quantization procedure changes. Specifically, the first interpretation can be seen as the common practice in machine learning to scale models to the dataset size.

Example 3.2 (Scaling Architecture). Let the number of parameters of our original models follow a scaling law (Hoffmann et al., 2022; Kaplan et al., 2020) f such that its number of parameters is: $f(n)$. Let the quantization method be fixed to a 1-bit quantization (mapping each parameter to its sign for instance). Then, following Example 2.2, for a dataset size n , the size of $\bar{\Theta}_n$ is $K_n = 2^{f(n)}$.

Under some mild assumptions outlined in Appendix A.3, we obtain the following result.

Theorem 3.3. *Assume that $\sqrt{n}\delta_2^n \rightarrow \infty$ and $\delta_2^n \rightarrow 0$.*

Then, we have

$$\lim_{n \rightarrow \infty} -\frac{1}{n(\delta_2^n)^2} \log(1 - \text{MIS}_n(P, \mathcal{A}_{\mathcal{Q}_n})) \geq \frac{1}{2\sigma^2}, \quad (4)$$

where $\sigma^2 = \max_k \lim_{n \rightarrow \infty} (\delta_2^n / \delta_k^n)^2 (\sigma_k^n)^2$.

For a size-adaptive Quantizer $\mathcal{Q} := (\mathcal{Q}_n)$, let $r_{\mathcal{Q}}^n := (\delta_2^n)^2 / (2\sigma^2)$ be the constant of Theorem 3.3 multiplied by the square of the minimal loss gap. Theorem 3.3 then stipulates that the MIS of a quantized algorithm, whose quantization \mathcal{Q} is Size-Adaptive, is of order $1 - e^{-nr_{\mathcal{Q}}^n(1+o(1))}$ which by hypothesis converges to 1 as n grows to infinity, ensuring asymptotic security. Furthermore, Theorem 3.3 suggests that for two size-adaptive Quantizers \mathcal{Q} and \mathcal{R} , $r_{\mathcal{Q}}^n \geq r_{\mathcal{R}}^n$ implies that $\mathcal{A}_{\mathcal{Q}}$ produces more secure parameters than $\mathcal{A}_{\mathcal{R}}$ (asymptotically). Theorem 3.3 then proposes to use $r_{\mathcal{Q}}^n$ as a measure to compare different quantizers. Most importantly, this quantity wholly relies upon the asymptotic expectations and variances of the random variables $\ell(\bar{\theta}_k^n, z) - \ell(\bar{\theta}_1^n, z)$.

Remark 3.4. The theoretical setting of subsection 3.2 encompasses modern architectures and habits of machine learning designs. This setting enables us to explicit the quantity $r_{\mathcal{Q}}^n$ controlling the asymptotic MIS of a quantized algorithm. The most vital point of Theorem 3.3 is that this result holds for all attacks, including currently unknown (and possibly more powerful) attacks. The following sections focus on empirically demonstrating that the estimate of $r_{\mathcal{Q}}^n$ is adequate to rank quantizers by their privacy level.

4. Estimating Quantized Algorithm Privacy

4.1. Measuring the privacy of quantized models

To estimate the security of an algorithm $\mathcal{A}_{\mathcal{Q}}$ using Theorem 3.3, we must compute the loss gaps δ_k^n between the best quantized model and all possible quantizers in $\bar{\Theta}$. However, this is computationally infeasible, as even a simple quantizer like 1-bit quantization leads to an exponentially large $\bar{\Theta}$ with respect to the number of parameters. We address this intractability by observing that only a few quantizers dominate the estimation of $r_{\mathcal{Q}}^n$. Specifically, $r_{\mathcal{Q}}^n$ depends on:

- The two lowest average quantized losses $m_{\bar{\theta}_1}$ and $m_{\bar{\theta}_2}$.
- The values $\lim_{n \rightarrow \infty} (\delta_2^n / \delta_k^n)^2 (\sigma_k^n)^2$ which measure the trade-off between the mean loss gap and the per-sample variance of quantized models.

Crucially, $\max_k \lim_{n \rightarrow \infty} (\delta_2^n / \delta_k^n)^2 (\sigma_k^n)^2$ is empirically dominated by low-loss quantizers (see subsection F.3), suggesting that exploring the entire set $\bar{\Theta}$ is unnecessary, as focusing on low-loss quantizers is sufficient to estimate $r_{\mathcal{Q}}^n$.

We thus propose estimating using quantized models derived from the training trajectory of θ_n . Since $\hat{\theta}_n$ is optimized to minimize ℓ , the quantizers with the lowest loss likely reside near this trajectory. This justifies our focus on the training trajectory, which efficiently captures critical quantizers. The complete procedure is outlined in Algorithm 1.

We propose an implementation of Algorithm 1 as a wrapper of Pytorch Lightning’s “LightningModule” class (Falcon & The PyTorch Lightning team, 2019), as well as the code to replicate all experiments.¹

Algorithm 1 Estimation of $r_{\mathcal{Q}}^n$

```

1: Input: A training dataset  $\mathcal{D}_n$ , a validation dataset  $\mathcal{D}_{\text{val}}$ ,
   a learning algorithm  $\mathcal{A}$ , a quantizer  $\mathcal{Q}$ , an initialized
   model  $\theta$ , a number of epochs  $K$ .
2: Output: An estimate of  $r_{\mathcal{Q}}^n$ .
3: Initialization: Set the list of all quantized loss  $\mathcal{L}_{\text{val}} = \{\}$ ,
   of all average quantized losses  $m_{\text{val}} = \{\}$ , and of
   all variances  $\sigma_{\text{val}}^2 = \{\}$ .
4: for  $k = 1$  to  $K$  do
5:    $\theta \leftarrow \mathcal{A}(\theta, \mathcal{D}_n)$ .
6:    $\bar{\theta} \leftarrow \mathcal{Q}(\theta)$ .
7:    $\mathcal{L}_k \leftarrow \{\ell(\bar{\theta}, z) : z \in \mathcal{D}_{\text{val}}\}$ .
8:    $m_k \leftarrow \frac{1}{|\mathcal{D}_{\text{val}}|} \sum_{z \in \mathcal{D}_{\text{val}}} \ell(\bar{\theta}, z)$ .
9:    $\mathcal{L}_{\text{val}}[k] \leftarrow \mathcal{L}_k$ .
10: end for
11:  $\text{idx} \leftarrow \text{argsort}(m_{\text{val}})$ .
12:  $m_{\text{val}} \leftarrow m_{\text{val}}[\text{idx}]$ .
13:  $\mathcal{L}_{\text{val}} \leftarrow \mathcal{L}_{\text{val}}[\text{idx}]$ .
14: for  $k = 2$  to  $K$  do
15:    $\sigma_{\text{val}}^2[k] \leftarrow \text{Var}(\mathcal{L}_{\text{val}}[k] - \mathcal{L}_{\text{val}}[1])$ .
16: end for
17:  $r_{\mathcal{Q}} \leftarrow \frac{1}{2} \left[ \max_{2 \leq k \leq K} \left( \sigma_{\text{val}}^2[k] \times \left( \frac{m_{\text{val}}[2] - m_{\text{val}}[1]}{m_{\text{val}}[k] - m_{\text{val}}[1]} \right)^2 \right) \right]^{-1}$ .
18: return  $r_{\mathcal{Q}}^n = r_{\mathcal{Q}}(m_{\text{val}}[2] - m_{\text{val}}[1])^2$ .

```

4.2. Baseline estimation of the MIS

Inferring membership of \tilde{z} by an MIA can naturally be considered as a statistical test,

$$\begin{cases} H_0 : & \text{“}\tilde{z} \text{ belongs to the training dataset”} \\ H_1 : & \text{“}\tilde{z} \text{ does not belong to the training dataset”} \end{cases}$$

Under the mathematical setting presented in Appendix A.1, these hypotheses can be apprehended as deciding whether $\hat{\theta}_n$ is independent or not to \tilde{z} . Specifically, testing H_0 against H_1 is equivalent to testing H'_0 against H'_1 , where

$$\begin{cases} H'_0 : & (\hat{\theta}_n, \tilde{z}) \sim P_{(\hat{\theta}_n, z_1)} \\ H'_1 : & (\hat{\theta}_n, \tilde{z}) \sim P_{\hat{\theta}_n} \otimes P. \end{cases} \quad (5)$$

For any dominating measure ζ on $P_{(\hat{\theta}_n, z_1)}$ (and $P_{\hat{\theta}_n} \otimes P$), denoting by f (resp. g) the density of $P_{(\hat{\theta}_n, z_1)}$ (resp. $P_{\hat{\theta}_n} \otimes P$) with respect to ζ , we have that $\phi^*(\theta, z) =$

¹https://anonymous.4open.science/r/Mol_Downstream-B3DB/README.md

$\mathbb{1} \left\{ \frac{f(\theta, z)}{g(\theta, z)} \geq 1 \right\}$ satisfies:

$$\sup_{\phi} \text{Acc}_n(\phi; P, \mathcal{A}) = \text{Acc}_n(\phi^*; P, \mathcal{A}). \quad (6)$$

The function ϕ^* is the Neyman-Pearson test for H'_0 against H'_1 . This suggests that evaluating empirically the MIS of an algorithm amounts down to training a discriminator, and evaluate it. The baseline approach therefore consists in training a binary classifier $g_{\psi} : \Theta \times \mathbb{R}^d \times \mathbb{R} \rightarrow [0, 1]$ to distinguish between samples z sampled from the training set of a given $\hat{\theta}_n$ and sampled from the product distribution $P_{\hat{\theta}_n} \otimes P$, and evaluate its accuracy. For a sample $z = (x, y) \sim P$, where $x \in \mathbb{R}^d$ is the input and y its corresponding label, and a model $\hat{\theta}_n$, the discriminator minimizes the binary cross-entropy loss:

$$\ell_{\text{DISC}}(\hat{\theta}_n, z) = \text{BinaryCE} \left(g_{\psi}(\hat{\theta}_n, x, y), \mathbb{1}_{z \in \mathcal{D}_{\text{train}}(\hat{\theta}_n)} \right),$$

where $\mathcal{D}_{\text{train}}(\hat{\theta}_n)$ is the training set of $\hat{\theta}_n$.

The discriminator is implemented as a feed-forward neural network that takes as input: x the input data, the flattened parameters of $\hat{\theta}_n$ and the loss of the model $\hat{\theta}_n$ on x, y . For instance, if the model $\hat{\theta}_n$ is a binary classifier, g_{ψ} is a neural network with input $x \in \mathbb{R}^d$, $\hat{\theta}_n$ and the binary cross-entropy loss of $\hat{\theta}_n$ on (x, y) .

We train the discriminator using a set of models, $\{\hat{\theta}_{n_i}\}_{i \in \{1, \dots, k_{\text{run}}\}}$ where each $\hat{\theta}_{n_i}$ is trained on an independent dataset $\{z_{i,1}, \dots, z_{i,n}\} \sim P$ of n i.i.d. samples. To generate negative samples, we independently sample additional sets, $z_{i,1}^{\text{neg}}, \dots, z_{i,n}^{\text{neg}} \sim P$, ensuring no overlap with the training sets of any models, or between the negative samples of different models. This independence between datasets is critical for preventing information leakage but may be restrictive in practice due to high data requirements.

A key drawback of this approach arises when $\hat{\theta}_n$ contains multiple layers. Different permutations of the weights of the hidden units can represent identical models, but the discriminator g_{ψ} , which relies on flattened parameters, is not invariant to such permutations.

5. Numerical Experiments

As we focus solely on ranking quantization procedures (Theorem 3.3 being asymptotic and potentially containing irrelevant constants), we omit specific $r_{\mathcal{Q}}^n$ values in the figures for clarity and readability.

5.1. Synthetic experiments

To confirm that our estimation of $r_{\mathcal{Q}}^n$ enables the ranking of quantization methods according to their level of privacy, we compare this ranking to the one obtained using the baseline

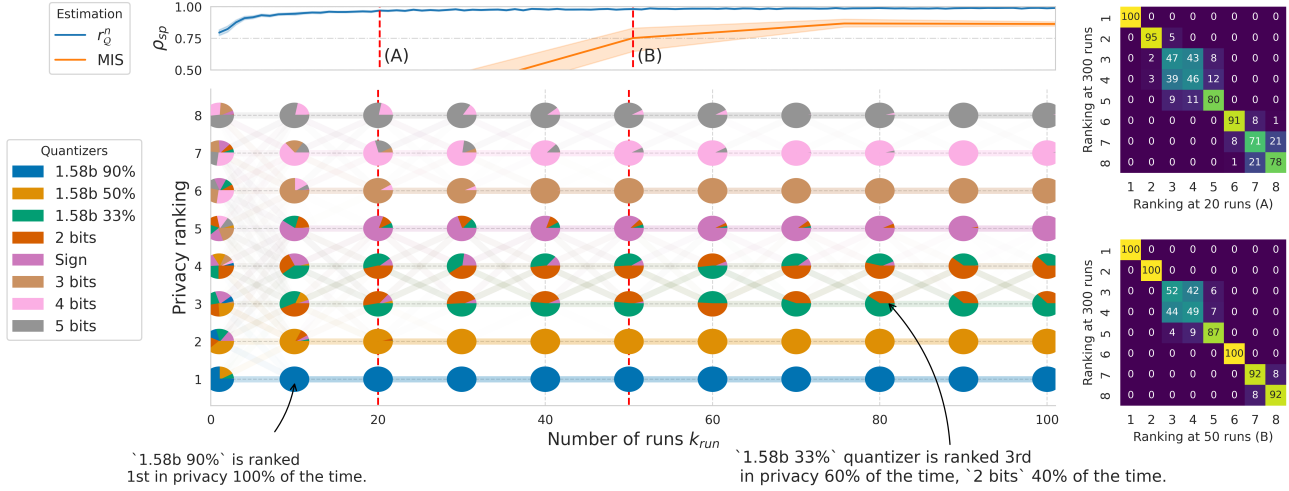


Figure 1: **Stability of Privacy rankings.** To obtain reliable estimates of r_Q^n , we average its value over multiple runs k_{run} (number of classifiers trained). The central plot illustrates how the rankings of quantizers, based on r_Q^n , evolve with the number of runs. Each column of pie charts represents the proportion of quantizers predicted at each rank (across 100 different subsets of k_{run} runs) with connecting lines showing shifts in predicted rankings. As the number of runs increases, the rankings stabilize, and when averaged over 50 runs, each quantizer is ranked at its final position 90% of the time (except for the 2 bits and 1.58b 33% quantizers). The top figure shows the evolution of the average Spearman correlation between r_Q^n (resp. the baseline’s estimation of the MIS) when evaluated over $k_{\text{run}} \leq 100$ and $k_{\text{run}} = 300$. The confusion matrices on the right compare rankings estimated using 300 runs to those obtained with 20 and 50 runs.

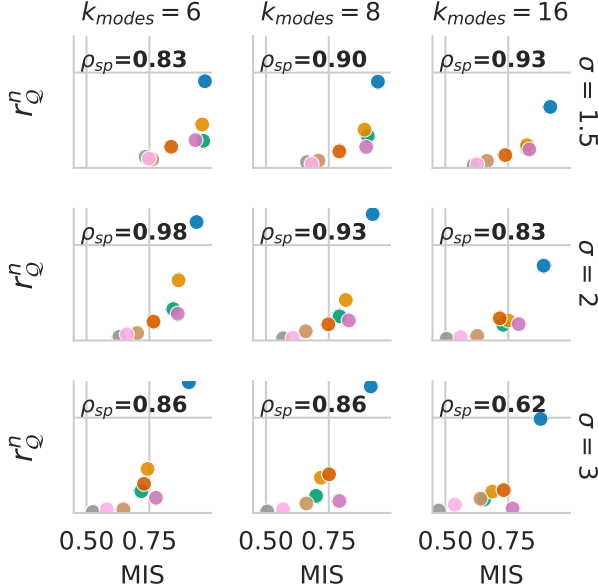


Figure 2: **Relationship between r_Q^n and the MIS.** Each sub-plot displays the estimated values of r_Q^n and the MIS for each quantizer under varying experimental configurations, with their corresponding Spearman correlation (ρ_{sp}). The strong correlations confirm that our method enables the comparison of different quantization techniques’ security.

estimation of the MIS. To perform this comparison, we rely on synthetic experiments, where we can train and evaluate a large number of classifiers, and ensure the independence between each classifier’s training set to train g_ψ .

5.1.1. EXPERIMENTAL SETUP

Datasets. We generate data points sampled from \mathbb{R}^{128} using $k_{\text{modes}} \in \{6, 8, 16\}$ isotropic Gaussian distributions with standard deviation $\sigma \in \{1.5, 2, 3\}$, where each cluster is assigned a label in $\{0, 1\}$.

Classifiers. As mentioned above, the baseline estimation method is limited to models consisting of a single layer. Consequently, all classifiers in our experiments are single-layer fully connected networks. To increase the expressivity of these networks, the input features are augmented with x^2 (element-wise squared features). Each classifier is trained on $n = 128$ samples for 3000 epochs using the Adam optimizer with a learning rate of 10^{-4} . To evaluate our approach, we train $k_{\text{run}} = 300$ classifiers (θ) on each distribution, with each run involving new i.i.d. samples, and we investigate in Figure 1 the impact of k_{run} on our evaluation of the quantizers’ privacy.

Quantization. For our experiments, we consider a range of different quantization methods, including: 1bit quantization by taking the sign of the weights (Sign), 1.58 bits

quantization with different sparsity levels ($1.58b \{x\}\%$ where $x\%$ of the weights with the smallest magnitude are set to zero, and the rest to their sign), and quantization on 2, 3, 4, and 5 bits. A detailed description of the quantization methods is provided in [Appendix D](#).

5.1.2. VALIDATION OF THE APPROACH

Estimation of the privacy guarantees. [Figure 2](#) illustrates the correlation between our proposed metric r_Q^n and the MIS baseline. We observe that our metric effectively quantifies the privacy of quantized models: higher values correspond to greater MIS. We report the Spearman correlation between both metrics (the correlation between the rankings induced by both metrics), and as expected, quantizers with more bits of information, such as 5 bits and 4 bits, are the least private across all datasets. In contrast, the $1.58b \ 90\%$ quantizer, which introduces 90% sparsity by setting weights to zero, achieves the highest privacy. Interestingly, the `Sign` method, which quantizes weights to 1 bit, is less private than the $1.58b \ 33\%$ quantizer, despite using fewer bits. This behavior aligns with observations from the baseline method, suggesting that sparsity plays a more significant role in privacy than the number of bits alone. Overall, the rankings produced by r_Q^n closely match those of the baseline method, with an average Spearman correlation of $\rho_{sp} = 0.86$, demonstrating that r_Q^n reliably ranks quantization methods by their privacy levels.

Quantizer ranking stability. While our experiments compute r_Q^n by averaging over 300 runs, such extensive computation may be impractical for real-world deployment due to resource constraints. [Figure 1](#) shows how the stability of r_Q^n -based rankings improves as the number of runs increases. Critically, the ranking of the most and least private quantizers stabilizes early: after just 20 runs, the 5 bits quantizer is consistently ranked least private, followed by 4 bits and 3 bits, while $1.58b \ 90\%$ (highest sparsity) remains the most private, followed by $1.58b \ 50\%$.

Computational cost. All experiments were conducted on NVIDIA A6000 GPUs with 48GB of memory. The estimation of r_Q^n introduces a small computational overhead during model training, as it requires computing the quantized model’s loss at each validation step, often for multiple quantization processes, adding approximately 1s to the training time of one $\hat{\theta}_n$ (4m total). In contrast, the baseline MIS estimation requires training multiple classifiers ($\hat{\theta}_n$) to train the discriminator g_ψ , which can also be sensitive to the hyperparameter choice, resulting in significant computational and data demands. The top figure of [Figure 1](#) shows that the rankings obtained with the r_Q^n -based approach stabilizes close to the final ranking after only 20 runs, as demonstrated with Spearman correlations over 0.95, while the MIS’s base-

line estimation does not reach this threshold until 150 runs. As a result, ranking quantizers using r_Q^n ($\approx 1h$) is significantly faster than using the baseline MIS method ($\approx 10h$).

5.2. Experiments on molecular datasets

5.2.1. EXPERIMENTAL SETUP

In our second experimental setting, we analyze a real-world application: molecular modeling. In the field of drug discovery, data is an invaluable and highly sensitive asset, and determining whether predictive models might inadvertently leak proprietary data is therefore highly valuable.

Pretrained Embedders. To generate one-dimensional molecular embeddings, we evaluate four pretrained models from the representation learning literature: GraphMVP (Liu et al., 2022a) and 3D-Infomax (Stärk et al., 2021) (3D-2D mutual information maximization), MolR (Wang et al., 2022) (reaction-aware pretraining), and ChemBERTa-MTR (Ahmad et al., 2022) (multitask regression with SMILES tokenization). The embeddings are passed to small feed-forward networks for downstream tasks, and we quantify the privacy impact of each embedder in [Appendix F](#).

Downstream tasks. We evaluate and train the models on various property prediction tasks from the Therapeutic Data Commons (TDC) platform (Huang et al., 2021), focusing on ADMET properties (Absorption, Distribution, Metabolism, Excretion, and Toxicity). These tasks encompass both binary classification and regression problems with datasets of varying sizes and complexities. For classification tasks, we report the AUC-ROC scores, and for regression tasks, we report R2 scores (coefficient of determination). For both metrics, higher values indicate better performance, with 1 being the maximum value for both metrics. For the regression tasks, the R2 score can be negative, indicating that the model performs worse than a simple mean prediction.

Task models. For each downstream task, we train fully connected networks (two layers, hidden dimension 128) for 500 epochs. To ensure robust estimation of r_Q^n , we allocate 40% of the dataset to the validation set. Each experiment is repeated 10 times, with 90% of the training set randomly subsampled in each run to ensure different training trajectories are used. We quantify the impact of quantization on performance measuring the relative performance of the quantized model to the original: for a metric m (AUROC or R2): $r_m^{\text{val}} = m_{\text{quantized}}^{\text{val}} / m_{\text{original}}^{\text{val}}$. Full results, including performance-privacy trade-offs grouped by embedders, are available in [Appendix F](#).

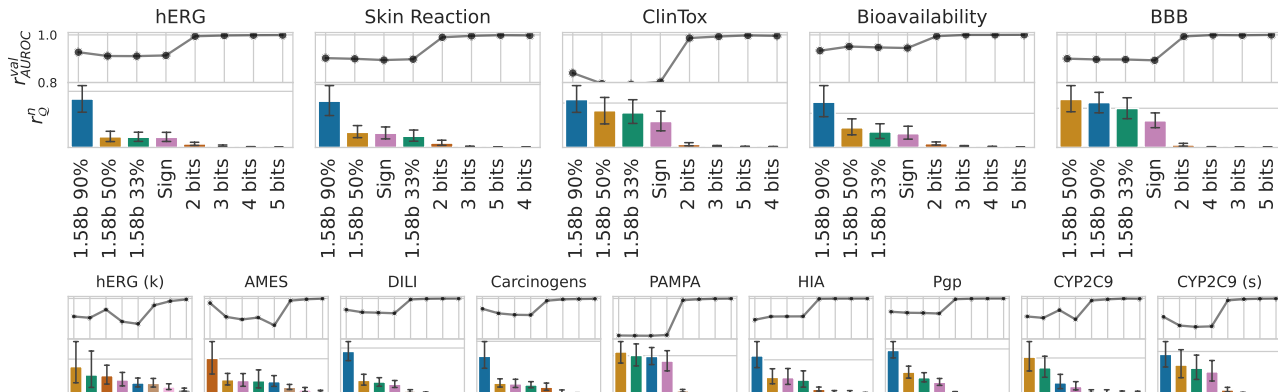


Figure 3: **Impact of quantization on classification tasks.** Evolution of the privacy of each downstream model r_Q^n along with relative performances of the quantized models compared to the original on classification task.

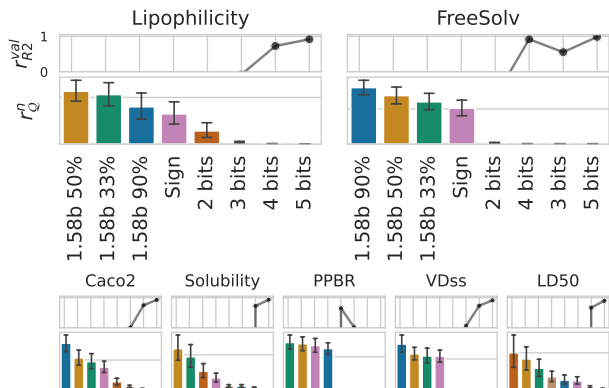


Figure 4: **Impact of quantization on regression tasks.** Evolution of the privacy of each downstream model r_Q^n along with relative performances of the quantized models compared to the original on regression task.

5.2.2. PRIVACY-PERFORMANCE TRADE-OFF

Classification tasks. Figure 3 illustrates the trade-off between privacy (r_Q^n) and relative performance (r_{AUROC}^{val}) for classification tasks. We identify two regimes: (1) for high values of r_Q^n , the quantized models achieve high privacy (e.g., 1.58b 90%), but the performances are significantly lower than the original models ($r_{AUROC}^{val} \approx 90\%$), in particular on ClinTox (Gayvert et al., 2016) (toxicity prediction) and PAMPA_NCATS (Siramshetty et al., 2021) (membrane permeability) where r_{AUROC}^{val} goes down to 80%. (2) Low-privacy quantizers (2 - 5 bits) preserve near-original performance but are consistently ranked least private. Across almost all datasets, the 1.58b 90% quantizer appears to be the most secure, while obtaining better performance than other sparse quantizers, notably on ClinTox, Carcinogens_Lagunin (Lagunin et al., 2009), and CYP2C9 substrate classification (Carbon-Mangels & Hutter, 2011).

Regression tasks. For regression tasks (see Figure 4), quantization introduces a stark privacy-performance imbalance. Unlike classification, even moderately aggressive quantization (e.g., 2 bits) results in negative R2 scores, indicating worse-than-baseline predictions (even though the direct predictions are not accurate, we show in the subsection F.1 the ordering of the predictions is preserved). Only non-private quantizers (4 - 5 bits) achieve R2 scores comparable to original models. This disparity arises because regression requires precise weight values to estimate continuous targets, whereas classification relies on decision boundaries that are more robust to quantization. Consequently, regression tasks lack a viable privacy-performance trade-off: quantizers either degrade performance catastrophically or retain performance at the cost of privacy. This underscores the need for novel quantization strategies tailored to regression.

6. Discussions and Limitations

In this work, we investigated the privacy of quantization procedures for machine learning models, particularly their vulnerability to data leakage. We established a theoretical foundation by proving that, for both fixed and adaptive model-quantization procedures, the Membership Inference Security (MIS) of the learning algorithm is asymptotically determined by the distribution of the quantized models’ loss per sample. We introduced a methodology for comparing quantization procedures in terms of privacy, with limited computational cost. Through extensive experiments on both synthetic and real-world datasets, we validated the effectiveness of our approach and explored the privacy-performance trade-offs of quantization in molecular property prediction, highlighting the practical implications of our findings.

Our study has some limitations. Since our analysis focuses on evaluating a training procedure rather than individual trained models, it does not directly predict the security of a

specific trained model. Additionally, due to computational constraints, we concentrated on Post-Training Quantization (PTQ) and did not examine Quantization-Aware Training (QAT), which presents a potential direction for future research. Specifically, we aim to explore QAT, where $r_{\mathcal{Q}}^n$ could be jointly optimized with the loss function.

7. Impact Statement

Our work focuses on the evaluation of the privacy of quantization procedures, which could help secure these models, thereby making it possible to share them more broadly while mitigating privacy risks for users and data contributors. More generally, this paper presents work whose goal is to advance the field of Machine Learning. There are many potential societal consequences of our work, none which we feel must be specifically highlighted here.

References

- Ahmad, W., Simon, E., Chithrananda, S., Grand, G., and Ramsundar, B. Chemberta-2: Towards chemical foundation models, 2022.
- Araujo, A. and Giné, E. The central limit theorem for real and banach valued random variables. (*No Title*), 1980.
- Aubinais, E., Gassiat, E., and Piantanida, P. Fundamental limits of membership inference attacks on machine learning models. *arXiv preprint arXiv:2310.13786*, 2023.
- Balaskas, K., Karatzas, A., Sad, C., Siozios, K., Anagnostopoulos, I., Zervakis, G., and Henkel, J. Hardware-aware dnn compression via diverse pruning and mixed-precision quantization. *IEEE Transactions on Emerging Topics in Computing*, 12(4):1079–1092, 2024.
- Banner, R., Hubara, I., Hoffer, E., and Soudry, D. Scalable methods for 8-bit training of neural networks. *Advances in neural information processing systems*, 31, 2018.
- Bengio, Y., Léonard, N., and Courville, A. Estimating or propagating gradients through stochastic neurons for conditional computation. *arXiv preprint arXiv:1308.3432*, 2013.
- Carbon-Mangels, M. and Hutter, M. C. Selecting Relevant Descriptors for Classification by Bayesian Estimates: A Comparison with Decision Trees and Support Vector Machines Approaches for Disparate Data Sets. *Molecular Informatics*, 30(10):885–895, 2011. ISSN 1868-1751. doi: 10.1002/minf.201100069. URL <https://onlinelibrary.wiley.com/doi/abs/10.1002/minf.201100069>.
- Carlini, N., Chien, S., Nasr, M., Song, S., Terzis, A., and Tramer, F. Membership inference attacks from first principles. In *2022 IEEE Symposium on Security and Privacy (SP)*, pp. 1897–1914. IEEE, 2022.
- Carlini, N., Hayes, J., Nasr, M., Jagielski, M., Sehwag, V., Tramer, F., Balle, B., Ippolito, D., and Wallace, E. Extracting training data from diffusion models. In *32nd USENIX Security Symposium (USENIX Security 23)*, pp. 5253–5270, 2023.
- Chaudhuri, K., Guo, C., and Rabbat, M. Privacy-aware compression for federated data analysis. In Cussens, J. and Zhang, K. (eds.), *Proceedings of the Thirty-Eighth Conference on Uncertainty in Artificial Intelligence*, volume 180 of *Proceedings of Machine Learning Research*, pp. 296–306. PMLR, 01–05 Aug 2022. URL <https://proceedings.mlr.press/v180/chaudhuri22a.html>.
- De Acosta, A. Moderate deviations and associated laplace approximations for sums of independent random vectors. *Transactions of the American Mathematical Society*, 329(1):357–375, 1992.
- Del Grosso, G., Pichler, G., Palamidessi, C., and Piantanida, P. Bounding information leakage in machine learning. *Neurocomputing*, 534:1–17, 2023.
- Dembo, A. *Large deviations techniques and applications*. Springer, 2009.
- Falcon, W. and The PyTorch Lightning team. PyTorch Lightning, March 2019. URL <https://github.com/Lightning-AI/lightning>.
- Famili, A. and Lao, Y. Deep neural network quantization framework for effective defense against membership inference attacks. *Sensors*, 23(18), 2023. ISSN 1424-8220. doi: 10.3390/s23187722. URL <https://www.mdpi.com/1424-8220/23/18/7722>.
- Gayvert, K. M., Madhukar, N. S., and Elemento, O. A Data-Driven Approach to Predicting Successes and Failures of Clinical Trials. *Cell Chemical Biology*, 23(10):1294–1301, October 2016. ISSN 2451-9448. doi: 10.1016/j.chembiol.2016.07.023.
- Gersho, A. and Gray, R. M. *Vector Quantization and Signal Compression*. Kluwer Academic Publishers, 1992. ISBN 9780792391814. URL <http://www.worldcat.org/isbn/9780792391814>.
- Gholami, A., Kim, S., Dong, Z., Yao, Z., Mahoney, M. W., and Keutzer, K. A survey of quantization methods for efficient neural network inference. In *Low-Power Computer Vision*, pp. 291–326. Chapman and Hall/CRC, 2022.
- Gong, R., Ding, Y., Wang, Z., Lv, C., Zheng, X., Du, J., Qin, H., Guo, J., Magno, M., and Liu, X. A survey of low-bit large language models: Basics, systems, and algorithms. *arXiv preprint arXiv:2409.16694*, 2024.
- Gupta, U., Stripelis, D., Lam, P. K., Thompson, P., Ambite, J. L., and Ver Steeg, G. Membership inference attacks on deep regression models for neuroimaging. In *Medical Imaging with Deep Learning*, pp. 228–251. PMLR, 2021.

- Hartley, J. and Tsafaris, S. A. Measuring unintended memorisation of unique private features in neural networks. *arXiv preprint arXiv:2202.08099*, 2022.
- Hayes, J., Melis, L., Danezis, G., and De Cristofaro, E. L. Membership inference attacks against generative models; 2018. URL <https://api.semanticscholar.org/CorpusID/202588705>.
- Hoffmann, J., Borgeaud, S., Mensch, A., Buchatskaya, E., Cai, T., Rutherford, E., de Las Casas, D., Hendricks, L. A., Welbl, J., Clark, A., Hennigan, T., Noland, E., Millican, K., van den Driessche, G., Damoc, B., Guy, A., Osindero, S., Simonyan, K., Elsen, E., Rae, J. W., Vinyals, O., and Sifre, L. Training compute-optimal large language models, 2022. URL <https://arxiv.org/abs/2203.15556>.
- Hu, H., Salicic, Z., Sun, L., Dobbie, G., Yu, P. S., and Zhang, X. Membership inference attacks on machine learning: A survey. *ACM Computing Surveys (CSUR)*, 54(11s):1–37, 2022.
- Huang, K., Fu, T., Gao, W., Zhao, Y., Roohani, Y., Leskovec, J., Coley, C. W., Xiao, C., Sun, J., and Zitnik, M. Therapeutics data commons: Machine learning datasets and tasks for drug discovery and development. *Proceedings of Neural Information Processing Systems, NeurIPS Datasets and Benchmarks*, 2021.
- Jacob, B., Kligys, S., Chen, B., Zhu, M., Tang, M., Howard, A., Adam, H., and Kalenichenko, D. Quantization and training of neural networks for efficient integer-arithmetic-only inference. In *Proceedings of the IEEE conference on computer vision and pattern recognition*, pp. 2704–2713, 2018.
- Kaplan, J., McCandlish, S., Henighan, T., Brown, T. B., Chess, B., Child, R., Gray, S., Radford, A., Wu, J., and Amodei, D. Scaling laws for neural language models, 2020. URL <https://arxiv.org/abs/2001.08361>.
- Kowalski, C., Famili, A., and Lao, Y. Towards Model Quantization on the Resilience Against Membership Inference Attacks. In *2022 IEEE International Conference on Image Processing (ICIP)*, pp. 3646–3650, October 2022. doi: 10.1109/ICIP46576.2022.9897681. URL <https://ieeexplore.ieee.org/document/9897681>. ISSN: 2381-8549.
- Lagunin, A., Filimonov, D., Zakharov, A., Xie, W., Huang, Y., Zhu, F., Shen, T., Yao, J., and Poroikov, V. Computer-Aided Prediction of Rodent Carcinogenicity by PASS and CISOC-PSCT. *QSAR & Combinatorial Science*, 28(8): 806–810, 2009. ISSN 1611-0218. doi: 10.1002/qsar.200860192.
- Lin, J., Tang, J., Tang, H., Yang, S., Chen, W.-M., Wang, W.-C., Xiao, G., Dang, X., Gan, C., and Han, S. Awq: Activation-aware weight quantization for on-device llm compression and acceleration. *Proceedings of Machine Learning and Systems*, 6:87–100, 2024.
- Liu, S., Wang, H., Liu, W., Lasenby, J., Guo, H., and Tang, J. Pre-training molecular graph representation with 3d geometry. In *International Conference on Learning Representations*, 2022a. URL <https://openreview.net/forum?id=xQUelpOKPam>.
- Liu, Y., Wen, R., He, X., Salem, A., Zhang, Z., Backes, M., De Cristofaro, E., Fritz, M., and Zhang, Y. {ML-Doctor}: Holistic risk assessment of inference attacks against machine learning models. In *31st USENIX Security Symposium (USENIX Security 22)*, pp. 4525–4542, 2022b.
- Ma, L., Sun, M., and Shen, Z. Fbi-llm: Scaling up fully binarized llms from scratch via autoregressive distillation. *arXiv preprint arXiv:2407.07093*, 2024a.
- Ma, S., Wang, H., Ma, L., Wang, L., Wang, W., Huang, S., Dong, L., Wang, R., Xue, J., and Wei, F. The era of 1-bit llms: All large language models are in 1.58 bits, 2024b. URL <https://arxiv.org/abs/2402.17764>.
- Murakonda, S. K. and Shokri, R. Ml privacy meter: Aiding regulatory compliance by quantifying the privacy risks of machine learning. *arXiv preprint arXiv:2007.09339*, 2020.
- Nagel, M., Baalen, M. v., Blankevoort, T., and Welling, M. Data-free quantization through weight equalization and bias correction. In *Proceedings of the IEEE/CVF International Conference on Computer Vision*, pp. 1325–1334, 2019.
- Nagel, M., Fournarakis, M., Amjad, R. A., Bondarenko, Y., Van Baalen, M., and Blankevoort, T. A white paper on neural network quantization. *arXiv preprint arXiv:2106.08295*, 2021.
- Nagel, M., Fournarakis, M., Bondarenko, Y., and Blankevoort, T. Overcoming oscillations in quantization-aware training. In *International Conference on Machine Learning*, pp. 16318–16330. PMLR, 2022.
- Pang, J., Cai, T., Zhang, B., Wu, J., and Tao, Y. Push quantization-aware training toward full precision performances via consistency regularization. *arXiv preprint arXiv:2402.13497*, 2024.
- Sablayrolles, A., Douze, M., Schmid, C., Ollivier, Y., and Jégou, H. White-box vs black-box: Bayes optimal strategies for membership inference. In *International Conference on Machine Learning*, pp. 5558–5567. PMLR, 2019.

- Shokri, R., Stronati, M., Song, C., and Shmatikov, V. Membership inference attacks against machine learning models. In *2017 IEEE symposium on security and privacy (SP)*, pp. 3–18. IEEE, 2017.
- Siramshetty, V., Williams, J., Nguyen, D.-T., Neyra, J., Southall, N., Mathé, E., Xu, X., and Shah, P. Validating adme qsar models using marketed drugs. *SLAS DISCOVERY: Advancing the Science of Drug Discovery*, 26(10):1326–1336, 2021. doi: 10.1177/24725552211017520. URL <https://doi.org/10.1177/24725552211017520>. PMID: 34176369.
- Song, C. and Raghunathan, A. Information leakage in embedding models. In *Proceedings of the 2020 ACM SIGSAC conference on computer and communications security*, pp. 377–390, 2020.
- Song, C., Ristenpart, T., and Shmatikov, V. Machine learning models that remember too much. In *Proceedings of the 2017 ACM SIGSAC Conference on computer and communications security*, pp. 587–601, 2017.
- Staab, R., Vero, M., Balunović, M., and Vechev, M. Beyond memorization: Violating privacy via inference with large language models. *arXiv preprint arXiv:2310.07298*, 2023.
- Stärk, H., Beaini, D., Corso, G., Tossou, P., Dallago, C., Günemann, S., and Liò, P. 3d infomax improves gnn for molecular property prediction. *arXiv preprint arXiv:2110.04126*, 2021.
- Villard, J. and Piantanida, P. Secure multiterminal source coding with side information at the eavesdropper. *IEEE Transactions on Information Theory*, 59(6):3668–3692, 2013. doi: 10.1109/TIT.2013.2245394.
- Wang, H., Li, W., Jin, X., Cho, K., Ji, H., Han, J., and Burke, M. D. Chemical-reaction-aware molecule representation learning. In *International Conference on Learning Representations*, 2022. URL <https://openreview.net/forum?id=6sh3pIzKS->.
- Wang, H., Ma, S., Dong, L., Huang, S., Wang, H., Ma, L., Yang, F., Wang, R., Wu, Y., and Wei, F. Bitnet: Scaling 1-bit transformers for large language models. *arXiv preprint arXiv:2310.11453*, 2023.
- Wang, H., Fu, W., Tang, Y., Chen, Z., Huang, Y., Piao, J., Gao, C., Xu, F., Jiang, T., and Li, Y. A survey on responsible llms: Inherent risk, malicious use, and mitigation strategy. *arXiv preprint arXiv:2501.09431*, 2025.
- Wang, L., Ma, L., Cao, S., Zhang, Q., Xue, J., Shi, Y., Zheng, N., Miao, Z., Yang, F., Cao, T., et al. Ladder: Enabling efficient {Low-Precision} deep learning computing through hardware-aware tensor transformation. In *18th USENIX Symposium on Operating Systems Design and Implementation (OSDI 24)*, pp. 307–323, 2024.
- Yan, G., Li, T., Wu, K., and Song, L. Killing two birds with one stone: Quantization achieves privacy in distributed learning. *Digital Signal Processing*, 146:104353, 2024. ISSN 1051-2004. doi: <https://doi.org/10.1016/j.dsp.2023.104353>. URL <https://www.sciencedirect.com/science/article/pii/S1051200423004487>.
- Youn, Y., Hu, Z., Ziani, J., and Abernethy, J. Randomized quantization is all you need for differential privacy in federated learning, 2023. URL <https://arxiv.org/abs/2306.11913>.
- Yuan, Z., Zhou, R., Wang, H., He, L., Ye, Y., and Sun, L. Vit-1.58 b: Mobile vision transformers in the 1-bit era. *arXiv preprint arXiv:2406.18051*, 2024.
- Zeng, C., Liu, S., Xie, Y., Liu, H., Wang, X., Wei, M., Yang, S., Chen, F., and Mei, X. Abq-llm: Arbitrary-bit quantized inference acceleration for large language models. *arXiv preprint arXiv:2408.08554*, 2024.
- Zhu, X., Li, J., Liu, Y., Ma, C., and Wang, W. A survey on model compression for large language models. *Transactions of the Association for Computational Linguistics*, 12:1556–1577, 2024.

A. Additional Assumptions and Notations

A.1. Mathematical Setting

We give here the mathematical setting for the theoretical results of [section 3](#) and [section 4](#) to hold. Specifically, we use the mathematical setting of ([Aubinais et al., 2023](#)). We redefine an MIA as follows.

Definition A.1 (MIA). Any measurable map $\phi : \Theta \times \mathcal{Z} \rightarrow \{0, 1\}$ is considered to be a *Membership Inference Attack*.

Here we have encoded *member* by 1. We define a test point \tilde{z} as follows. Let $T \in \{0, 1\}$ be a Bernoulli random variable with parameter $1/2$. Let $z_0 \sim P$ and U be a random variable whose distribution is \hat{P}_n conditionally to the training dataset \mathcal{D}_n , where T, z_0 and U are independent. Additionally, z_0 and T are independent of \mathcal{D}_n . We define the test point by,

$$\tilde{z} := TU + (1 - T)z_0. \quad (7)$$

This definition is a formalization of the fact that a test point is either a member of the training dataset ($T = 1$) or not a member ($T = 0$). The random variable z_0 is used as a placeholder to represent the non-member property of the test point. With this framework, the following relation holds,

Theorem A.2 (([Aubinais et al., 2023](#))). *For any distribution P and any algorithm \mathcal{A} , we have*

$$MIS_n(P, \mathcal{A}) = 1 - \|P_{(\hat{\theta}_n, z_1)} - P_{\hat{\theta}_n} \otimes P\|_{TV}, \quad (8)$$

where $\|\nu_1 - \nu_2\|_{TV}$ is the total variation distance between the distributions ν_1 and ν_2 .

A.2. Fixed Quantizer

We denote by $L_{k,j} := \ell(\bar{\theta}_k, z_j) - \ell(\bar{\theta}_1, z_j)$ the random loss gap between $\bar{\theta}_k$ and $\bar{\theta}_1$ evaluated on z_j , whose expectation is $\delta_k := \mathbb{E}[L_{k,j}]$. We additionally denote by $D := \text{diag}((\delta_k)_{k>1})$ the diagonal **loss gaps matrix**. We give the additional hypotheses for [Theorem 3.1](#).

- **H1.1.** We have $\mathbb{E}\left[e^{<t, D^{-1}[L_{k,1} - \delta_k]_{k>1}>}\right] < \infty$ for all t in a neighborhood of $0 \in \mathbb{R}^{K-1}$.
- **H1.2.** The minimal loss gap satisfies $\delta_2 > 0$.

A sufficient (albeit non-necessary) condition for H1.1 to hold is that the loss function l is bounded. Specifically, the hypothesis H1.1 is sufficient for the constant of [Theorem 3.1](#) to be strictly positive. If for all $t \neq 0$ we have $\mathbb{E}\left[e^{<t, D^{-1}[L_{k,1} - \delta_k]_{k>1}>}\right] = \infty$, then the theorem becomes trivial as we would have $C_P^1 = 0$. The hypothesis H1.2 implies that the loss gaps matrix D is invertible.

A.3. Size-Adaptive Quantizers

We give here additional notations and hypotheses for [Theorem 3.3](#). Let $\bar{\Theta}_n := \{\bar{\theta}_1^n, \dots, \bar{\theta}_{K_n}^n\}$ be the image of the Size-Adaptive Quantizer \mathcal{Q}_n , where K_n may or may not depend on n . Based on the assumptions given in [Theorem 3.3](#), assume without loss of generality that for all $n \in \mathbb{N}$, $m_{\bar{\theta}_1^n} < \dots < m_{\bar{\theta}_{K_n}^n}$. We recall that the **loss gaps** are defined as $\delta_k^n = m_{\bar{\theta}_k^n} - m_{\bar{\theta}_1^n}$ and the **loss variabilities** as $(\sigma_k^n)^2 := \text{Var}\left(L_{k,1}^n\right)$ where $L_{k,j}^n := \ell(\bar{\theta}_k^n, z_j) - \ell(\bar{\theta}_1^n, z_j)$. We set $D^n := \text{diag}((\delta_k^n)_{k>1})$. We will use the following hypotheses

- **H2.1.** The limits $\sigma_k^2 = \lim_{n \rightarrow \infty} \text{Var}(L_{k,1}^n)$ and $c_k = \lim_{n \rightarrow \infty} \frac{\delta_2^n}{\delta_k^n}$ exist.
- **H2.2.** We have $\sup_n \mathbb{E}\left[\exp\left(t \left\| \left(\frac{\delta_2^n}{\delta_k^n} L_{k,1}^n \right)_{1 < k \leq K_n} \right\|_2\right)\right] < \infty$, for all $t > 0$.
- **H2.3.** There exists $K < \infty$ such that for all $k > K$, $c_k^2 \sigma_k^2 = 0$.

- **H2.4.** The sequence of random variables $\left(\left(\frac{\delta_2^n}{\delta_k^n} L_{k,1}^n \right)_{1 < k \leq K_n} \right)_n$ is tight when canonically seen as a sequence in $l_2(\mathbb{R})$.

By definition, for all k , we have $\delta_2^n / \delta_k^n \in [0, 1]$. If the loss function ℓ is bounded, then the loss variabilities $(\sigma_k^n)^2$ are bounded as well. The hypothesis H2.1 is then only a light hypothesis.

A sufficient condition for H2.3 to hold is that there exists (asymptotically) finitely many global minima of the function l . Indeed, if there exists (asymptotically) finitely many global minima of the function ℓ , say K , this means that for all $k > K$, we have $\delta_k^n \xrightarrow[n \rightarrow \infty]{} 0$, whereas $\delta_2^n \xrightarrow[n \rightarrow \infty]{} 0$ resulting in $c_k = 0$ and H2.3. The value $K - 1$ corresponds to the intrinsic dimension of the asymptotic random variables $((\delta_2^n / \delta_k^n) L_{k,1}^n)_{1 < k \leq K_n}$.

The hypotheses presented in [Theorem 3.3](#), i.e. $\sqrt{n}\delta_2^n \xrightarrow[n \rightarrow \infty]{} \infty$ and $\delta_2^n \xrightarrow[n \rightarrow \infty]{} 0$, ensure that the loss gaps matrix D^n is invertible.

B. Preliminary Results

We give here preliminary results for the proof of the main theorem.

Lemma B.1. *Let $K \geq 2$, $a, b \in (0, 1)$. Let P and Q be two distributions over $\{1, \dots, K\}$ satisfying $P(1) = 1 - a$ and $Q(1) = 1 - b$. Then, we have*

$$|a - b| \leq \|P - Q\|_{TV} \leq \frac{|a - b| + a + b}{2}.$$

Lemma B.2. *Let M be a $J \times J$ square matrix and $j \in \{1, \dots, J\}$. Assume that $M_{-j,-j}$ and $M_{j,j} - M_{j,-j} [M_{-j,-j}]^{-1} M_{-j,j}$ are invertible, where $M_{-j,-j}$ is the sub-matrix of M consisting of all entries except the j^{th} row and column and $M_{-j,j}$ is the j^{th} column of M except its j^{th} entry. Then we have*

$$(M^{-1})_{j,j} = \left(M_{j,j} - M_{j,-j} [M_{-j,-j}]^{-1} M_{-j,j} \right)^{-1}$$

Proof of Lemma B.1. By definition, we have

$$\begin{aligned} \|P - Q\|_{TV} &= \frac{1}{2} \sum_{j=1}^K |p_j - q_j| \\ &= \frac{1}{2} |a - b| + \frac{1}{2} \sum_{j=2}^K |p_j - q_j|. \end{aligned}$$

By construction, we have $\sum_{j=2}^K p_j = a$ and $\sum_{j=2}^K q_j = b$. It is easy to see check that

$$\begin{aligned} \min \sum_{j=2}^K |p_j - q_j| &= |a - b|, \\ \max \sum_{j=2}^K |p_j - q_j| &= a + b, \end{aligned}$$

where the minimum and the maximum are taken over all distributions satisfying the condition over p_1 and q_1 , which concludes the proof. □

Proof of Lemma B.2. First note that if M is designed by block as follows,

$$M = \begin{pmatrix} A & B \\ C & D \end{pmatrix},$$

then we have

$$M^{-1} = \begin{pmatrix} (A - BD^{-1}C)^{-1} & * \\ * & * \end{pmatrix}, \quad (9)$$

as long as C and $A - BD^{-1}C$ are invertible. Let P_j and Q_j be $J \times J$ matrices defined for all j such that $P_j M$ permutes the first and the j^{th} rows of M , and $Q_j M$ permutes the $(j-1)^{\text{th}}$ and the j^{th} rows of M . For instance, if $J = 4$ and $j = 3$ then we have

$$P_3 = \begin{pmatrix} 0 & 0 & 1 & 0 \\ 0 & 1 & 0 & 0 \\ 1 & 0 & 0 & 0 \\ 0 & 0 & 0 & 1 \end{pmatrix}, \quad Q_3 = \begin{pmatrix} 1 & 0 & 0 & 0 \\ 0 & 0 & 1 & 0 \\ 0 & 1 & 0 & 0 \\ 0 & 0 & 0 & 1 \end{pmatrix}.$$

Note that we have $(P_j)^{-1} = P_j$ and $(Q_j)^{-1} = Q_j$. Let $R = Q_3 Q_4 \cdots Q_j P_j M P_j Q_j \cdots Q_4 Q_3$. Developing the formula, we get

$$R = \begin{pmatrix} M_{j,j} & M_{j,-j} \\ M_{-j,j} & M_{-j,-j} \end{pmatrix}. \quad (10)$$

On one hand, using Equation 9 and Equation 10, we have $R^{-1} = \begin{pmatrix} (M_{j,j} - M_{j,-j} [M_{-j,-j}]^{-1} M_{-j,j})^{-1} & * \\ * & * \end{pmatrix}$. On the other hand, distributing the inverse operator on the product of matrices and using again Equation 9, we have

$$\begin{aligned} R^{-1} &= Q_3 Q_4 \cdots Q_j P_j M^{-1} P_j Q_j \cdots Q_4 Q_3 \\ &= \begin{pmatrix} (M^{-1})_{j,j} & * \\ * & * \end{pmatrix}, \end{aligned}$$

which concludes the proof. \square

C. Main Theorems

This section is dedicated to the proof of the following theorems. Let denote by $\Delta_n(P, \mathcal{A}_{\mathcal{Q}}) := 1 - \text{MIS}_n(P, \mathcal{A}_{\mathcal{Q}})$ the quantity of interest for which Theorem 3.1 and Theorem 3.3 give asymptotic results. From Equation 8, we restate Theorem 3.1 and Theorem 3.3 as follows.

Theorem C.1 (Theorem 3.1). *Let \mathcal{Q} be a fixed quantizer. We assume H1.1 and H1.2. Then, we have*

$$\lim_{n \rightarrow \infty} \frac{1}{n} \log \Delta_n(P, \mathcal{A}_{\mathcal{Q}}) \leq - \inf_{x \in \Omega_{K-1}^c} \sup_{t \in \mathbb{R}^{K-1}} \left[\langle t, x \rangle - \log \mathbb{E} \left[e^{\langle t, D^{-1} [L_{k,j} - \delta_k]_{k>1} \rangle} \right] \right] < 0, \quad (11)$$

where $\Omega_{K-1} = [-1, \infty)^{K-1}$.

Theorem C.2 (Theorem 3.3). Let \mathcal{Q}_n be a Size-Adaptive quantizer. We assume H2.1, H2.2, H2.3 and H2.4. Assuming that $\lim_{n \rightarrow \infty} \delta_2^n = 0$ and $\lim_{n \rightarrow \infty} \sqrt{n} \delta_2^n = \infty$, we have

$$\lim_{n \rightarrow \infty} \frac{1}{n (\delta_2^n)^2} \log \Delta_n(P, \mathcal{A}_{\mathcal{Q}_n}) \leq -1/2\sigma^2. \quad (12)$$

We start by giving the proof of Theorem C.2 before Theorem C.1.

C.1. Proof of Theorem C.2

The proof of Theorem C.2 is immediate from Propositions C.3 and C.4 given below.

Proposition C.3. In the context of Theorem C.2, we have

$$\lim_{n \rightarrow \infty} \frac{1}{n (\delta_2^n)^2} \log \Delta_n(P, \mathcal{A}_{\mathcal{Q}_n}) \leq - \inf_{x \in \Omega^c} \frac{x^T \Lambda^+ x}{2}, \quad (13)$$

where Λ is defined as

$$\Lambda := \begin{pmatrix} \sigma_{2,2}^2 c_2^2 & \cdots & \sigma_{2,J}^2 c_2 c_K \\ \vdots & \ddots & \vdots \\ \sigma_{K,2}^2 c_K c_2 & \cdots & \sigma_{K,K}^2 c_K^2 \end{pmatrix},$$

where $\sigma_{k,l}^2 = \lim_{n \rightarrow \infty} \text{Cov}(L_{k,1}^n, L_{l,1}^n)$. The matrix Λ^+ is the Moore-Penrose pseudo-inverse Λ . Note that we have $\sigma_{k,k}^2 = \sigma_k^2$. The set Ω is given by $\Omega := [-1, \infty)^{K-1}$.

Proposition C.4. In the context of Proposition C.3, we have

$$\inf_{x \in \Omega^c} \frac{x^T \Lambda^+ x}{2} = 1/2\sigma^2. \quad (14)$$

Proof of Proposition C.3. Recall that $\hat{\theta}_n \sim \mathcal{A}_{\mathcal{Q}_n}(z_1, \dots, z_n)$. Note that from Equation 8 we have

$$\Delta_n(P, \mathcal{A}_{\mathcal{Q}_n}) = \mathbb{E} \left[\|\mathcal{L}(\hat{\theta}_n) - \mathcal{L}(\hat{\theta}_n | z_1)\|_{\text{TV}} \right], \quad (15)$$

where $\mathcal{L}(X)$ is the probability law of X , and the expectation is taken over z_1 . Letting $Z_k^n = \mathbb{P}(\hat{\theta}_n = \bar{\theta}_k^n | z_1)$ and $p_k^n = \mathbb{P}(\hat{\theta}_n = \bar{\theta}_k^n)$, we have

$$\begin{aligned} \Delta_n(P, \mathcal{A}_{\mathcal{Q}_n}) &= \frac{1}{2} \sum_{k=1}^{K_n} \mathbb{E} [|p_k^n - Z_k^n|] \\ &\leq \frac{\mathbb{E} [|p_1^n - Z_1^n|] + 2 - \mathbb{E} [p_1^n + Z_1^n]}{2} \\ &= \frac{\mathbb{E} [|p_1^n - Z_1^n|] + 2(1 - p_1^n)}{2} \\ &\leq \frac{2(1 - p_1^n) + 2(1 - p_1^n)}{2} \\ &= 2(1 - p_1^n), \end{aligned}$$

where the first inequality comes from Lemma B.1. By construction, $\mathcal{A}_{\mathcal{Q}_n}$ minimizes the empirical loss. Letting $\Omega_{K-1} = [-1, \infty)^{K-1}$, we then have

$$\begin{aligned}
 p_1^n &= \mathbb{P} \left(1 = \arg \min_k \left\{ \frac{1}{n} \sum_{j=1}^n \ell(\bar{\theta}_k^n, z_j) \right\} \right) \\
 &= \mathbb{P} \left(\forall k > 1, \frac{1}{n} \sum_{j=1}^n [\ell(\bar{\theta}_k^n, z_j) - \ell(\bar{\theta}_1^n, z_j)] \geq 0 \right) \\
 &= \mathbb{P} \left(\forall k > 1, \frac{1}{n} \sum_{j=1}^n [L_{k,j}^n - \delta_k^n] \geq -\delta_k^n \right) \\
 &= \mathbb{P} \left(\frac{1}{n} \sum_{j=1}^n [L_{k,j}^n - \delta_k^n]_{k>1} \in D^n \Omega_{K-1} \right) \\
 &= \mathbb{P} \left(\frac{1}{n\delta_2^n} \sum_{j=1}^n [(\delta_2^n)^{-1} D^n]^{-1} [L_{k,j}^n - \delta_k^n]_{k>1} \in \Omega_{K-1} \right),
 \end{aligned} \tag{16}$$

which gives

$$1 - p_1^n = \mathbb{P} \left(\frac{1}{n\delta_2^n} \sum_{j=1}^n [(\delta_2^n)^{-1} D^n]^{-1} [L_{k,j}^n - \delta_k^n]_{k>1} \in \Omega_{K-1}^c \right).$$

By H2.3, $[(\delta_2^n)^{-1} D^n]^{-1} [L_{k,j}^n - \delta_k^n]_{k>1}$ lives (asymptotically) in a $(K-1)$ -dimensional euclidean subspace. By H2.2 and H2.4, as we live in an Hilbert space, using (Araujo & Giné, 1980), we have $\mathcal{L} \left(\frac{1}{\sqrt{n}} \sum_{j=1}^n [(\delta_2^n)^{-1} D^n]^{-1} [L_{k,j}^n - \delta_k^n]_{k>1} \right) \xrightarrow{n \rightarrow \infty} \gamma := \mathcal{N}_{K-1}(0, \Lambda)$, where \mathcal{N}_{K-1} is the $(K-1)$ -dimensional Gaussian distribution. Now, using the fact that $\mathbb{E} [L_{k,j}^n] = \delta_k^n$, H2.2, H2.4 and convergence to a Gaussian measure, using Theorem 2.2 of (De Acosta, 1992), we get

$$\begin{aligned}
 \lim_{n \rightarrow \infty} \frac{1}{n(\delta_2^n)^2} \log(1 - p_1^n) &= - \inf_{x \in \Omega_{K-1}^c} \begin{cases} \frac{x^T \Lambda^+ x}{2} & , \text{if } x \in H_\gamma \\ \infty & , \text{otherwise} \end{cases} \\
 &= - \inf_{x \in \Omega^c} \frac{x^T \Lambda^+ x}{2},
 \end{aligned}$$

where H_γ is the Hilbert space associated with γ (see (De Acosta, 1992)). Hence the result. \square

Proof of Proposition C.4. Let $M = \Lambda^+$. Note that $\Omega^c = \{x \in \mathbb{R}^{K-1} : \exists j, x_j < -1\}$, giving

$$\inf_{x \in \Omega^c} x^T M x = \min_j \inf_{x_{-j} \in \mathbb{R}^{K-1} x_j < -1} \inf x^T M x,$$

where we write x_{-j} equals x where we omit its j^{th} entry. We then shall write

$$x^T M x = x_j^2 M_{j,j} + 2x_j x_{-j}^T M_{-j,j} + x_{-j}^T M_{-j,-j} x_{-j}.$$

The infimum must be reached on the frontier of the set, i.e. such that $x_j = -1$ for some j . Indeed assuming x in the interior of Ω^c , we have that $x_j > -1$ for some j . Then for any $1 < \alpha < |x_j|$, $x_j/\alpha < -1$ meaning that x/α still belongs to the interior of Ω^c . However, $(x/\alpha)^T M(x/\alpha) = \frac{1}{\alpha^2} x^T M x < x^T M x$, which shows that x was not optimal. For an optimal x , we then have

$$x^T M x = M_{j,j} - 2x_{-j}^T M_{-j,j} + x_{-j}^T M_{-j,-j} x_{-j}.$$

It is then sufficient to study the optimization problem over x_{-j} , which amounts down to the optimization of a quadratic function, whose minimum is then reached for x_{-j} satisfying

$$\begin{aligned} \nabla_{x_{-j}} (-2x_{-j}^T M_{-j,j} + x_{-j}^T M_{-j,-j} x_{-j}) &= 0 \\ \iff x_{-j} &= (M_{-j,-j})^{-1} M_{-j,j}, \end{aligned}$$

giving

$$\inf_{x_{-j} \in \mathbb{R}^{J-1}} \inf_{x_j < -1} x^T M x = M_{j,j} - M_{j,-j} (M_{-j,-j})^{-1} M_{-j,j}.$$

Applying Lemma B.2 concludes the proof. □

C.2. Proof of Theorem C.1

We give here the proof of Theorem C.1.

Proof of Theorem C.1. Following the same steps of the proof of Theorem C.2 up to Equation 16, we have by removing the superscripts n where needed,

$$\begin{aligned} p_1 &= P \left(\frac{1}{n} \sum_{j=1}^n [L_{k,j} - \delta_k]_{k>1} \in D\Omega_{K-1} \right) \\ &= P \left(\frac{1}{n} \sum_{j=1}^n D^{-1} [L_{k,j} - \delta_k]_{k>1} \in \Omega_{K-1} \right), \end{aligned}$$

giving

$$1 - p_1 = P \left(\frac{1}{n} \sum_{j=1}^n D^{-1} [L_{k,j} - \delta_k]_{k>1} \in \Omega_{K-1}^c \right).$$

From H1.1, the result follows immediately using Corollary 6.1.6 of (Dembo, 2009). □

D. Quantizations

In this section, we provide additional details on the quantization procedures used in our experiments. Table 1 summarizes the quantizers used in the experiments, and Figure 5 illustrates how the different functions used quantize the interval $[-1, 1]$.

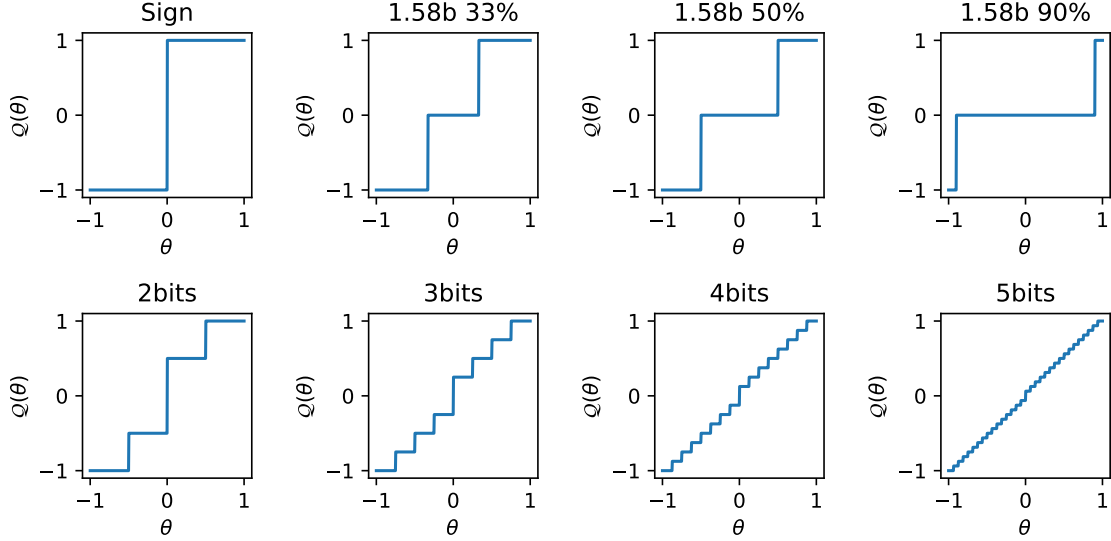

 Figure 5: Illustration of the quantization functions used on the interval $[-1, 1]$.

Table 1: Description of the quantizers used in the experiments.

quantizer	$\mathcal{Q}(\theta_j)$
Sign	$\mathcal{Q}(\theta_j) = \frac{\theta_j}{ \theta_j }$
1.58b 33%	$\mathcal{Q}(\theta_j) = \begin{cases} \frac{\theta_j}{ \theta_j }, & \text{if } \theta_j < q(\theta , 0.33) \\ 0, & \text{otherwise} \end{cases}$
1.58b 50%	$\mathcal{Q}(\theta_j) = \begin{cases} \frac{\theta_j}{ \theta_j }, & \text{if } \theta_j < q(\theta , 0.5) \\ 0, & \text{otherwise} \end{cases}$
1.58b 90%	$\mathcal{Q}(\theta_j) = \begin{cases} \frac{\theta_j}{ \theta_j }, & \text{if } \theta_j < q(\theta , 0.9) \\ 0, & \text{otherwise} \end{cases}$
2 bits	$\mathcal{Q}(\theta_j) = \frac{\theta_j}{ \theta_j } \frac{\alpha}{2} \times \text{int} \left(1 + \text{clip} \left(\frac{2\theta_j}{\alpha}, 0, 2 \right) \right), \quad \alpha = 2^{\text{round}(\log_2(\max \theta))}$
3 bit	$\mathcal{Q}(\theta_j) = \frac{\theta_j}{ \theta_j } \frac{\alpha}{4} \times \text{int} \left(1 + \text{clip} \left(\frac{4\theta_j}{\alpha}, 0, 4 \right) \right), \quad \alpha = 2^{\text{round}(\log_2(\max \theta))}$
4 bits	$\mathcal{Q}(\theta_j) = \frac{\theta_j}{ \theta_j } \frac{\alpha}{8} \times \text{int} \left(1 + \text{clip} \left(\frac{8\theta_j}{\alpha}, 0, 8 \right) \right), \quad \alpha = 2^{\text{round}(\log_2(\max \theta))}$
5 bits	$\mathcal{Q}(\theta_j) = \frac{\theta_j}{ \theta_j } \frac{\alpha}{16} \times \text{int} \left(1 + \text{clip} \left(\frac{16\theta_j}{\alpha}, 0, 16 \right) \right), \quad \alpha = 2^{\text{round}(\log_2(\max \theta))}$

E. Synthetic experiments

E.1. Trade-off between privacy and performance

In this section, we provide additional details on the synthetic experiments conducted to evaluate the trade-off between privacy and performance of quantized models. This trade-off is illustrated in Figure 6, where we plot the evolution of the quantification certificate r_Q^n with the model’s performance as the ratio of the original model’s training accuracy. We find that the trade-off between privacy and performance is less pronounced compared to the real-world experiments. In particular, while the least private quantizers do preserve most of the original performance, the more private quantizers seem to achieve similar performances on some data distribution (in particular, when $\sigma = 3$). This could be explained by the low performances of the trained models on such distributions as illustrated in Table 2. Furthermore, simple mixture of Gaussians might not be relevant to capture the complexity of real-world data distributions, and we therefore decided to focus our analysis of the performance-privacy trade-off on real-world applications.

E.2. Stability and Computational Complexity

As explained in subsection 4.2, the baseline approach consists in training a discriminator to distinguish between samples from the training set of a given $\hat{\theta}_n$ and samples from the product distribution $P_{\hat{\theta}_n} \otimes P$. Similarly the r_Q^n -based approach relies on the training of multiple models to average the values of r_Q^n obtained.

The computational overhead induced by the r_Q^n -based approach, namely computing the validation loss of the quantized models, is negligible compared to the total training time (1s against 4m). Similarly, the training of the discriminator takes only about 40m.

As a result, training multiple models $\hat{\theta}_n$ over multiple runs is the computational bottleneck of our privacy evaluations. To

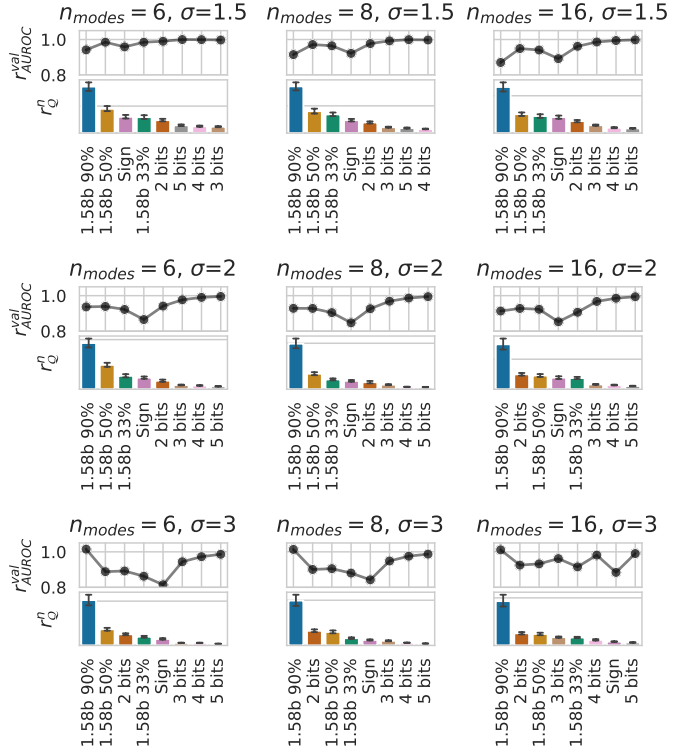


Figure 6: Evolution of r_Q^n with the quantized model’s performance as the ratio of the original model’s training accuracy (line) for various quantizers in our synthetic setup.

Table 2: Description of the quantizers used in the synthetic experiments.

σ	n_{modes}	Sign	1.58b 33%	1.58b 50%	2 bits	1.58b 90%	3 bits	4 bits	5 bits	Identity
1.5	6	0.954 (95%)	0.980 (98%)	0.981 (98%)	0.986 (99%)	0.938 (94%)	0.993 (99%)	0.995 (99%)	0.995 (100%)	0.996 (100%)
	8	0.904 (92%)	0.946 (96%)	0.953 (97%)	0.958 (97%)	0.897 (91%)	0.973 (99%)	0.978 (99%)	0.980 (99%)	0.981 (100%)
	16	0.825 (89%)	0.870 (94%)	0.878 (94%)	0.889 (96%)	0.805 (87%)	0.912 (98%)	0.920 (99%)	0.923 (99%)	0.925 (100%)
2	6	0.822 (86%)	0.876 (92%)	0.892 (93%)	0.894 (94%)	0.890 (93%)	0.928 (97%)	0.941 (99%)	0.945 (99%)	0.950 (100%)
	8	0.760 (84%)	0.811 (90%)	0.833 (92%)	0.831 (92%)	0.833 (92%)	0.869 (96%)	0.885 (98%)	0.892 (99%)	0.897 (100%)
	16	0.681 (85%)	0.724 (90%)	0.737 (92%)	0.741 (92%)	0.729 (91%)	0.772 (96%)	0.787 (98%)	0.793 (99%)	0.798 (100%)
3	6	0.625 (81%)	0.662 (86%)	0.681 (88%)	0.684 (89%)	0.779 (101%)	0.724 (94%)	0.746 (97%)	0.757 (98%)	0.767 (100%)
	8	0.595 (84%)	0.622 (88%)	0.639 (90%)	0.636 (90%)	0.716 (101%)	0.670 (94%)	0.689 (97%)	0.697 (98%)	0.706 (100%)
	16	0.555 (88%)	0.575 (91%)	0.585 (93%)	0.581 (92%)	0.635 (101%)	0.604 (96%)	0.616 (98%)	0.622 (99%)	0.628 (100%)

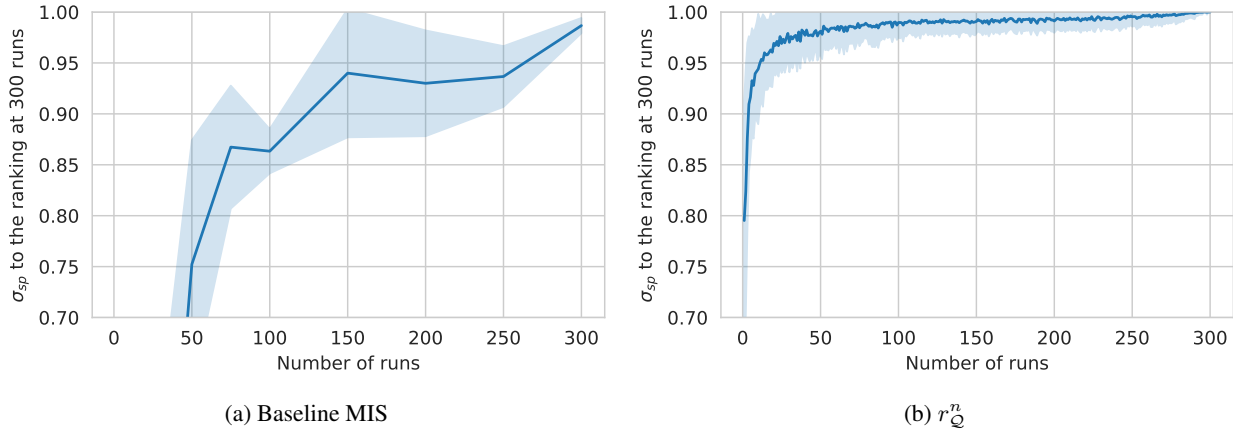


Figure 7: Correlation between the rankings obtained with the baseline MIS method (resp. r_Q^n) at a given number of run, with the ranking obtained with the baseline MIS method (resp. r_Q^n) at 300 runs.

properly evaluate the time required to obtain both rankings, one would have to answer the following question: 'How many runs do I need to launch to ensure the ranking I obtained is stable?'

Figure 7 shows how after 15 runs, the rankings obtained with r_Q^n are already highly correlated with the rankings obtained with 300 runs, while the rankings obtained with the baseline MIS method require 150 runs to reach the same level of correlation. As a result, the time required to obtain stable rankings with r_Q^n is significantly lower ($\approx 1h$) than with the baseline MIS method ($\approx 10h$).

E.3. Visualization of the datasets

We provide in Figure 8 a visualization of the synthetic datasets used in the experiments, through a PCA projection in dimension 2. This visualization helps understand how different data distribution might result in different empirical results, as some datasets are more challenging than others, such as the dataset with $n_{\text{cluster}} = 6$ and $\sigma = 1.5$, for whom the labels of the datapoints are easily separable, while $n_{\text{cluster}} = 16$ and $\sigma = 3$ provides a more challenging dataset, with overlapping clusters.

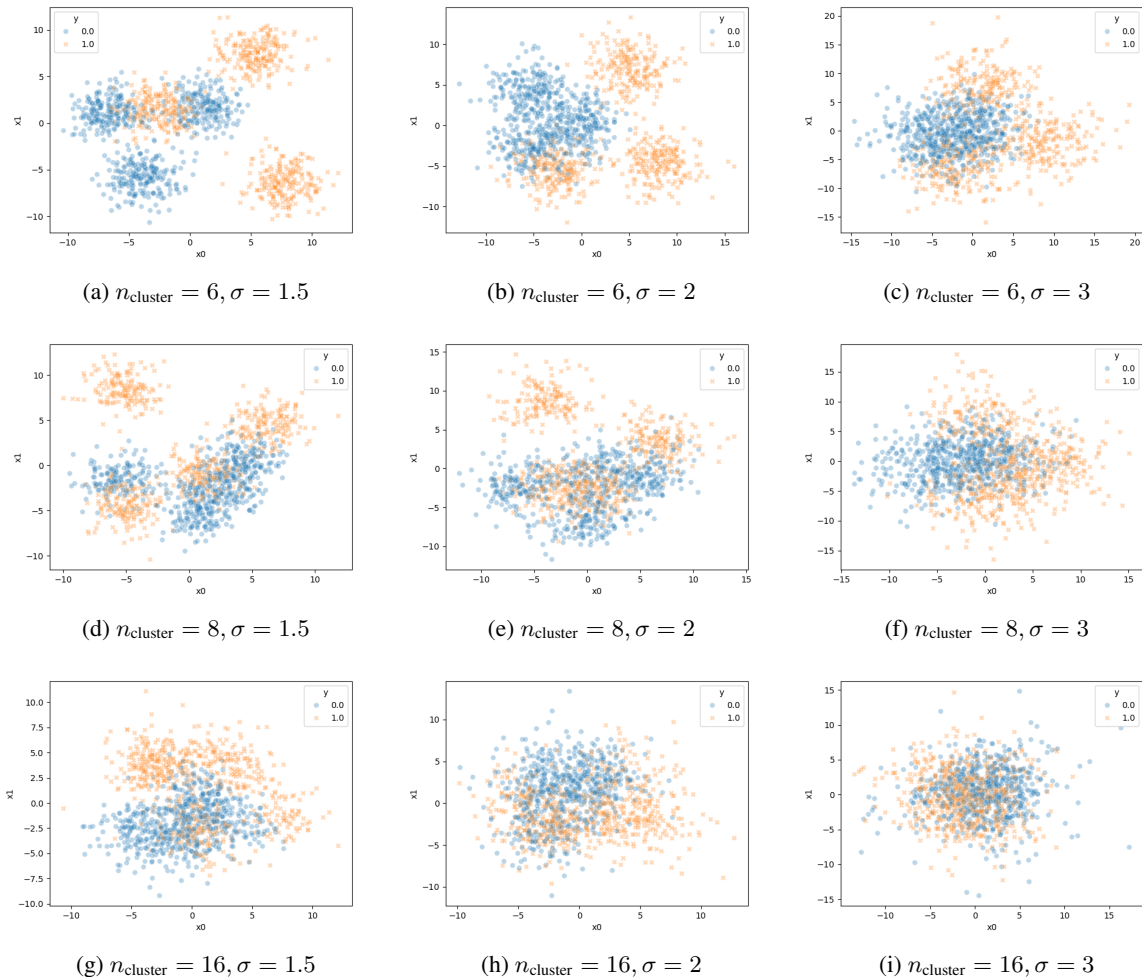


Figure 8: Visualization of the synthetic datasets used in the experiments, through a PCA projection in dimension 2 (the original space is \mathbb{R}^{128}).

F. Molecular experiments

F.1. Comprehensive results

We show in [Table 3](#) and [Table 4](#) the comprehensive results of the quantized models on the classification and regression tasks, respectively.

We observe that while the quantized models are generally less accurate than the original models, they still achieve reasonable performance on the classification tasks. On regression examples, the quantized models’ performances are significantly lower than the original models. In particular, when the quantization quantizes on less than 4 bits, the prediction of the molecular properties are almost consistently lower than a simple mean prediction. As explained in [subsection 5.2](#), this result is expected, as while classification tasks relies on the definition of boundary between classes, regression tasks require a fine-grained prediction of the target value.

However, while the direct predictions of the quantized models do not provide a good estimate of the target value, the ordering of the predictions is still preserved, as shown by the Spearman correlation between the quantized models’ predictions and the labels in [Table 5](#).

Table 3: AUROC performance of the quantized models on the classification tasks, averaged over all embedders.

dataset	Sign	1.58b 33%	1.58b 50%	1.58b 90%	2 bits	3 bits	4 bits	5 bits	original
AMES	0.773 (89%)	0.781 (90%)	0.784 (90%)	0.748 (86%)	0.843 (97%)	0.853 (98%)	0.859 (99%)	0.861 (99%)	0.862 (100%)
BBB Martins	0.800 (89%)	0.803 (89%)	0.807 (90%)	0.804 (89%)	0.890 (99%)	0.895 (99%)	0.895 (99%)	0.896 (100%)	0.896 (100%)
Bioavailability Ma	0.586 (94%)	0.588 (94%)	0.590 (95%)	0.579 (93%)	0.619 (99%)	0.622 (100%)	0.622 (100%)	0.623 (100%)	0.622 (100%)
CYP2C9 Substrate CarbonMangels	0.558 (86%)	0.557 (86%)	0.561 (86%)	0.589 (90%)	0.642 (99%)	0.646 (99%)	0.647 (99%)	0.647 (99%)	0.648 (100%)
CYP2C9 Veith	0.787 (89%)	0.793 (90%)	0.799 (91%)	0.827 (94%)	0.868 (99%)	0.873 (99%)	0.876 (99%)	0.877 (99%)	0.877 (100%)
Carcinogens Lagunin	0.766 (91%)	0.765 (91%)	0.772 (92%)	0.791 (94%)	0.824 (98%)	0.830 (99%)	0.831 (99%)	0.832 (99%)	0.833 (100%)
ClinTox	0.561 (80%)	0.555 (79%)	0.557 (79%)	0.589 (84%)	0.698 (98%)	0.702 (99%)	0.704 (99%)	0.706 (99%)	0.707 (100%)
DILI	0.827 (92%)	0.830 (93%)	0.831 (93%)	0.843 (94%)	0.888 (99%)	0.891 (99%)	0.892 (99%)	0.892 (99%)	0.892 (100%)
HIA Hou	0.805 (91%)	0.805 (91%)	0.804 (91%)	0.790 (89%)	0.882 (99%)	0.883 (99%)	0.883 (99%)	0.883 (100%)	0.883 (100%)
PAMPA NCATS	0.585 (81%)	0.583 (81%)	0.584 (81%)	0.583 (81%)	0.708 (99%)	0.711 (99%)	0.713 (99%)	0.714 (99%)	0.714 (100%)
Pgp Broccatelli	0.856 (92%)	0.858 (92%)	0.859 (92%)	0.864 (93%)	0.921 (99%)	0.924 (99%)	0.924 (100%)	0.924 (100%)	0.925 (100%)
Skin Reaction	0.664 (89%)	0.667 (89%)	0.668 (90%)	0.670 (90%)	0.735 (99%)	0.740 (99%)	0.741 (99%)	0.742 (99%)	0.743 (100%)
hERG	0.728 (91%)	0.726 (91%)	0.726 (91%)	0.739 (92%)	0.793 (99%)	0.795 (99%)	0.796 (99%)	0.797 (99%)	0.797 (100%)
hERG (k)	0.767 (88%)	0.783 (90%)	0.789 (91%)	0.757 (87%)	0.819 (94%)	0.837 (96%)	0.855 (98%)	0.862 (99%)	0.866 (100%)

 Table 4: R2 performance of the quantized models on the regression tasks, averaged over all embedders. If the R2 score is lesser than -1 , we display $-\text{inf}$ for clarity.

dataset	Sign	1.58b 33%	1.58b 50%	1.58b 90%	2 bits	3 bits	4 bits	5 bits	original
Caco2 Wang	$-\text{inf}$ ($-\text{inf}\%$)	$-\text{inf}$ ($-\text{inf}\%$)	$-\text{inf}$ ($-\text{inf}\%$)	$-\text{inf}$ ($-\text{inf}\%$)	$-\text{inf}$ (-364%)	0.008 (1%)	0.458 (75%)	0.567 (93%)	0.609 (100%)
HydrationFreeEnergy FreeSolv	$-\text{inf}$ ($-\text{inf}\%$)	$-\text{inf}$ ($-\text{inf}\%$)	$-\text{inf}$ ($-\text{inf}\%$)	$-\text{inf}$ ($-\text{inf}\%$)	-0.466 (-70%)	0.412 (55%)	0.669 (91%)	0.715 (98%)	0.725 (100%)
LD50 Zhu	$-\text{inf}$ ($-\text{inf}\%$)	$-\text{inf}$ ($-\text{inf}\%$)	$-\text{inf}$ ($-\text{inf}\%$)	$-\text{inf}$ ($-\text{inf}\%$)	$-\text{inf}$ (-578%)	-0.129 (-25%)	0.339 (67%)	0.454 (89%)	0.505 (100%)
Lipophilicity (az)	$-\text{inf}$ ($-\text{inf}\%$)	$-\text{inf}$ ($-\text{inf}\%$)	$-\text{inf}$ ($-\text{inf}\%$)	$-\text{inf}$ ($-\text{inf}\%$)	$-\text{inf}$ (-539%)	-0.037 (-7%)	0.404 (72%)	0.508 (91%)	0.552 (100%)
PPBR AZ	$-\text{inf}$ ($-\text{inf}\%$)	$-\text{inf}$ ($-\text{inf}\%$)	$-\text{inf}$ ($-\text{inf}\%$)	$-\text{inf}$ ($-\text{inf}\%$)	$-\text{inf}$ ($-\text{inf}\%$)	-0.480 (-233%)	0.022 (2%)	0.156 (65%)	0.229 (100%)
Solubility AqSolDB	$-\text{inf}$ ($-\text{inf}\%$)	$-\text{inf}$ ($-\text{inf}\%$)	$-\text{inf}$ ($-\text{inf}\%$)	$-\text{inf}$ ($-\text{inf}\%$)	$-\text{inf}$ (-792%)	-0.081 (-10%)	0.575 (72%)	0.740 (93%)	0.792 (100%)
VDss Lombardo	$-\text{inf}$ ($-\text{inf}\%$)	$-\text{inf}$ ($-\text{inf}\%$)	$-\text{inf}$ ($-\text{inf}\%$)	$-\text{inf}$ ($-\text{inf}\%$)	-0.859 (-287%)	-0.010 (6%)	0.175 (73%)	0.224 (91%)	0.248 (100%)

Table 5: Spearman correlations between the labels and the predictions of the quantized models on the regression tasks, averaged over all embedders.

dataset	Sign	1.58b 33%	1.58b 50%	1.58b 90%	2 bits	3 bits	4 bits	5 bits	original
Caco2 Wang	0.673 (89%)	0.713 (95%)	0.720 (95%)	0.679 (90%)	0.690 (92%)	0.733 (97%)	0.745 (99%)	0.748 (99%)	0.750 (100%)
HydrationFreeEnergy FreeSolv	0.905 (98%)	0.907 (99%)	0.906 (98%)	0.893 (97%)	0.910 (99%)	0.913 (99%)	0.915 (99%)	0.916 (99%)	0.916 (100%)
LD50 Zhu	0.572 (83%)	0.611 (89%)	0.618 (90%)	0.533 (77%)	0.596 (87%)	0.636 (92%)	0.669 (97%)	0.679 (99%)	0.685 (100%)
Lipophilicity (az)	0.658 (87%)	0.700 (92%)	0.705 (93%)	0.637 (84%)	0.669 (88%)	0.713 (94%)	0.741 (98%)	0.749 (99%)	0.754 (100%)
PPBR AZ	0.561 (98%)	0.563 (98%)	0.564 (99%)	0.555 (97%)	0.565 (99%)	0.568 (99%)	0.569 (99%)	0.570 (99%)	0.570 (100%)
Solubility AqSolDB	0.838 (94%)	0.853 (96%)	0.852 (96%)	0.756 (85%)	0.842 (94%)	0.864 (97%)	0.879 (99%)	0.884 (99%)	0.887 (100%)
VDss Lombardo	0.570 (99%)	0.572 (99%)	0.572 (99%)	0.560 (97%)	0.572 (99%)	0.573 (99%)	0.575 (99%)	0.575 (99%)	0.576 (100%)

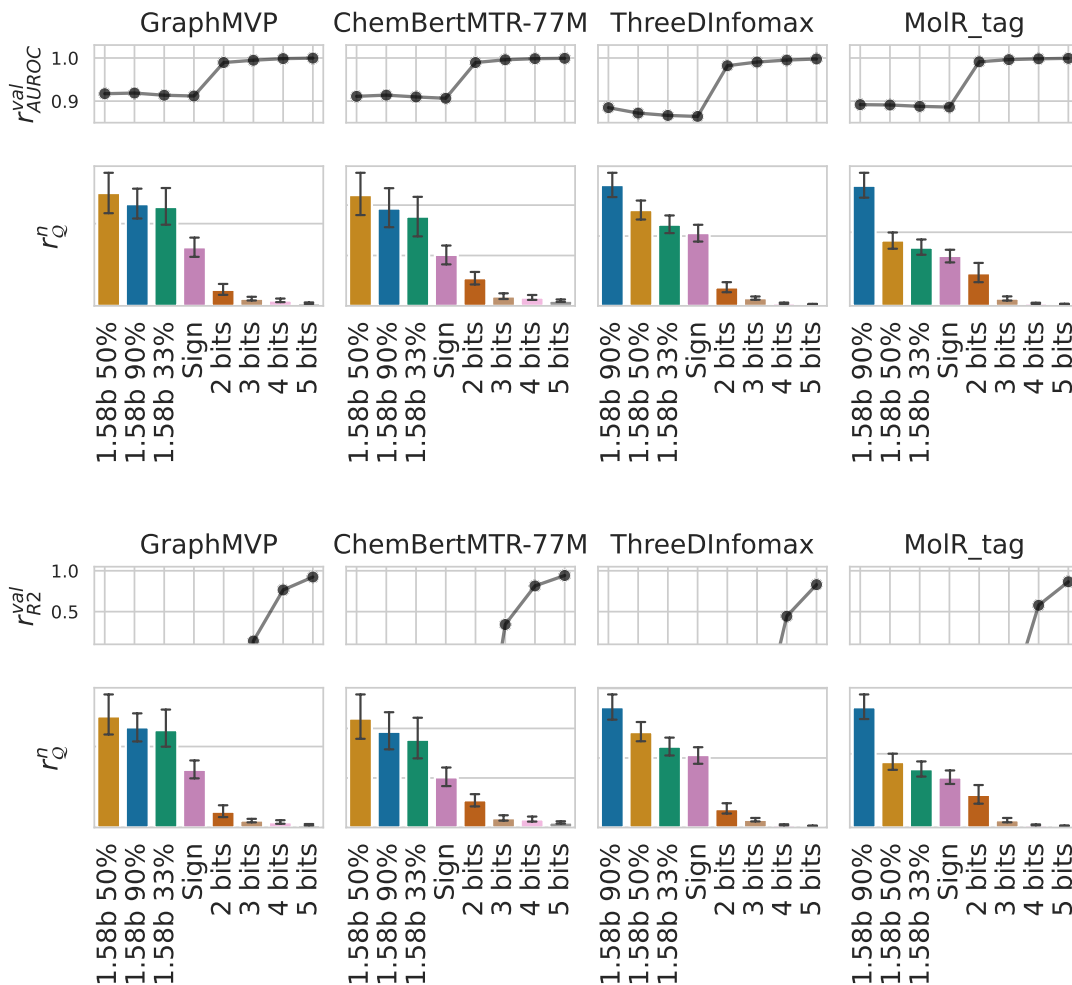


Figure 9: Evolution of the privacy of each downstream model r_Q^n along with relative performances of the quantized models compared to the original for each pretrained embedder. As the privacy of the model decreases, the performances of the quantized model increase, showing the trade-off between security and downstream performance.

F.2. Embedder privacy

Figure 9 shows the evolution of the privacy of each downstream model r_Q^n along with relative performances of the quantized models compared to the original for each pretrained embedder. For every pretrained embedder, we see no significant difference in the quantizers' privacy ranking, or in the trade-off between security and downstream performance.

F.3. Details on the evaluation of the quantizers' privacy

Our hypothesis in the estimation of r_Q^n is that the quantized weights with the lowest average loss dominate the maximum value of $\lambda_k = \Lambda_{k,k} = \lim_{n \rightarrow \infty} (\delta_2^n / \delta_k^n)^2 (\sigma_k^n)^2$. We show in Figure 10 the evolution of $\Lambda_{k,k}$ with the k , where the indexes are sorted with decreasing values of average loss, and the histogram of the index of the maximum value of $\Lambda_{k,k}$ for each quantizer, on 4 different datasets (trained on 500 epochs, hence $k \leq 500$). The maximum value of $\Lambda_{k,k}$ is indeed consistently reached on low k values, which seems to confirm our hypothesis, validating our sampling strategy for the estimation of r_Q^n .

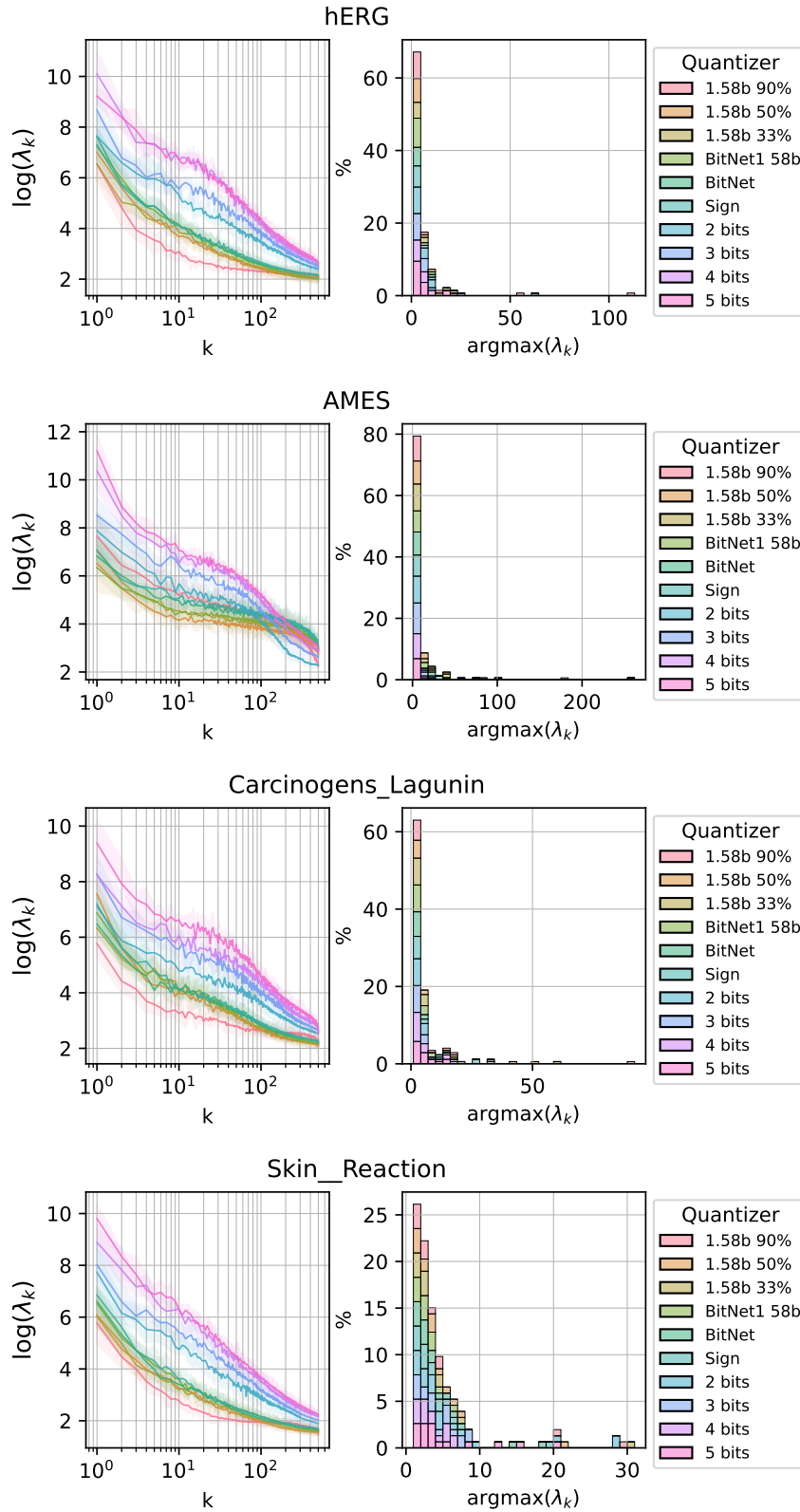


Figure 10: Evolution of $\Lambda_{k,k}$ with the k , where the indexes are sorted with decreasing values of average loss, and the histogram of the index of the maximum value of $\Lambda_{k,k}$ for each quantizer.